Neuronatin regulates pancreatic beta cell insulin content and secretion

Steven J. Millership[1, 2], Gabriela Da Silva Xavier[3], Agharul I. Choudhury[1], Sergio Bertazzo[4], Pauline Chabosseau[3], Silvia M. A. Pedroni[1, 2], Elaine E. Irvine[1], Alex Montoya[1], Peter Faull[1, 12], William R. Taylor[5], Julie Kerr-Conte[6], Francois Pattou[6], Jorge Ferrer[7], Mark Christian[8, 13], Rosalind M. John[9], Mathieu Latreille[1], Ming Liu[10], Guy A. Rutter[3], James Scott[11] and Dominic J. Withers[1, 2]

[1]MRC London Institute of Medical Sciences, Du Cane Road, London, W12 0NN, UK

[2]Institute of Clinical Sciences, Faculty of Medicine, Imperial College London, Du Cane Road, London, W12 0NN, UK

[3]Section of Cell Biology and Functional Genomics, Division of Diabetes, Endocrinology and Metabolism, Department of Medicine, Imperial College London, Du Cane Road, London, W12 0NN, UK

[4]Department of Medical Physics & Biomedical Engineering, University College London, Gower Street, London, WC1E 6BT, UK

[5]Computational Cell and Molecular Biology Lab, Francis Crick Institute, Midland Road, London, NW1 1AT, UK

[6]European Genomic Institute for Diabetes, UMR 1190 Translational Research for Diabetes, INSERM, CHU Lille, University of Lille, Lille, 59000 France

[7]Beta Cell Genome Regulation Lab, Department of Medicine, Imperial College London, Du Cane Road, London, W12 0NN, UK

[8]Institute of Reproductive and Developmental Biology, Department of Surgery and Cancer, Imperial College London, Du Cane Road, London, W12 0NN, UK

[9]School of Biosciences, Cardiff University, Museum Avenue, Cardiff, CF10 3AX, UK

[10]Department of Endocrinology and Metabolism, Tianjin Medical University General Hospital, 154 Anshan Road, Heping District, Tianjin, 300052, China

[11]National Heart and Lung Institute, Department of Medicine, Imperial College London, Du Cane Road, London, W12 0NN, UK

[12]Current Address: Mass Spectrometry Proteomics Platform, Francis Crick Institute, Midland Road, London, NW1 1AT, UK

[13]Current Address: Division of Biomedical Sciences, Warwick Medical School, University of Warwick, Coventry, CV4 7AL, UK

Correspondence:

Dominic J. Withers, Institute of Clinical Sciences, Faculty of Medicine, Imperial College London, Du Cane Road, London, W12 0NN, UK

Tel: +44 02083 833014

E-mail: d.withers@imperial.ac.uk

Conflict of interest

The authors have declared that no conflict of interest exists.

Summary

Neuronatin (*Nnat*) is an imprinted gene implicated in human obesity and widely expressed in neuroendocrine and metabolic tissues in a hormone and nutrient-sensitive manner. However, its molecular and cellular functions and precise role in organismal physiology remain only partly defined. Here we demonstrate that mice lacking *Nnat* globally or specifically in beta cells display profound impairment of glucose-stimulated insulin secretion leading to defective glucose handling under conditions of nutrient-excess. In contrast, we report no evidence for any feeding or body weight phenotypes in global *Nnat* null mice. At the molecular level neuronatin augments insulin signal peptide cleavage by binding to the signal peptidase complex and facilitates translocation of the nascent preprohormone. Loss of neuronatin expression in beta cells therefore reduces insulin content and blunts glucose-stimulated insulin secretion. NNAT expression in turn is glucose-regulated and therefore this mechanism represents a novel site of nutrient-sensitive control of beta cell function and whole animal glucose homeostasis. These data also suggest a potential wider role for *Nnat* in the regulation of metabolism through the modulation of peptide processing events.

Introduction

Imprinted genes display monoallelic expression according to parent of origin due to epigenetic events initiated in the germline (1). Around 150 such genes have been identified in mice with about 50% of these also found in humans. Although its origins remain obscure, mouse and human genetic studies have revealed key roles for genomic imprinting in regulating both development and various aspects of post-natal physiology. For example, many imprinted genes regulate placental function, fetal and neonatal growth and early life metabolism and behaviour (2). Furthermore, a number of human syndromes with fetal and post-natal growth and metabolic phenotypes such as Prader-Willi, Angelman and Beckwith-Wiedemann syndromes result from abnormalities in the expression of specific imprinted genes (2). Despite these advances, for a majority of imprinted genes, the precise cellular and molecular mechanisms through which their effects on growth and metabolism are mediated remain unclear.

Neuronatin (*Nnat*) is a paternally expressed imprinted proteolipid gene originally identified in the developing rat brain but also found in all placental mammals including humans. It is expressed predominantly in the neuroendocrine systems of the developing fetus and adult but is also found in adipose tissue (3-5). The *Nnat* locus resides in a 'microimprinted' region within the intronic sequence of the neighboring gene *Blcap*, with differential expression controlled by localised methylation of the silenced maternal allele (6-10). *In vivo* studies have shown that *Nnat* expression is dynamically regulated by nutrient status. For example, fasting and leptin administration down- and up-regulate *Nnat* mRNA levels in the hypothalamus, respectively (11-13). Nutrient-dependent changes in expression are also seen in white

adipose tissue and pancreatic beta cells and altered expression is found in the adipose tissue and islets of rodent models of obesity and diabetes (5, 14-16). Furthermore, recent evidence suggests that in mice *Nnat* expression, together with a cluster of other imprinted genes under the regulation of the chromatin interacting protein *Trim28*, underpins the "stochastic" development of obesity seen in inbred mouse strains (17). Single nucleotide polymorphisms in the human *NNAT* locus are associated with extreme childhood obesity, and reduced *NNAT* expression has been reported in the adipose tissue of obese children (13, 17). Together these findings suggest a role for neuronatin in the regulation of body weight and the pathophysiology of obesity, although the potential underlying molecular mechanisms for these observations remain undetermined.

While to date no direct *in vivo* evidence has been demonstrated for a role for *Nnat* in the regulation of glucose homeostasis, *in vitro* studies manipulating its expression in cultured pancreatic beta cells suggest that *Nnat* may regulate glucose-stimulated insulin secretion (GSIS) (14, 18). In terms of potential mechanisms underlying this observation, *in vitro* studies have shown that NNAT is present in the endoplasmic reticulum (ER) (14, 19) and, in part due to a suggested structural resemblance to the calcium-handling protein phospholamban, have implicated this protein in the control of intracellular calcium dynamics (3, 5, 14, 20). Involvement in the control of ion channels, Ca^{2+} ATPases and glucokinase have also been proposed (21).

Despite the above evidence implicating *Nnat* in the control of GSIS, a defined molecular and cellular mechanism that might underpin this role has yet to be defined. Furthermore, as no detailed characterization of an *Nnat* deficient mouse model has

been previously described, the precise *in vivo* functions of *Nnat*, with respect to pancreatic islet function and specifically to the distinct events regulating GSIS, remain unclear.

Here, we reveal that *in vivo* deletion of *Nnat* either globally or specifically in beta cells causes defective GSIS, leading to impaired glucose intolerance under conditions of nutrient overload. Thus, *Nnat* is required for normal pancreatic beta cell insulin secretion. In contrast we find little evidence for any feeding or body weight phenotypes in global *Nnat* null mice. We further demonstrate that NNAT binds to the signal peptidase complex (SPC) and facilitates the translocation of nascent preproinsulin into the ER. Impairment of preproinsulin signal peptide (SP) cleavage in beta cells leads to a deficiency of available mature insulin secretory granules and defective GSIS. Neuronatin expression itself is regulated by glucose and so together, these studies identify a novel component of the insulin processing apparatus, illustrate the important contribution of the SPC to the molecular events involved in the control of GSIS, and thus define a previously unrecognized site of nutrient-sensitive control of beta cell function and whole animal glucose homeostasis. Our studies also suggest a potentially wider role for *Nnat* in the regulation of a range of peptide secretory processes relevant to growth and metabolism.

Results

Mice with targeted deletion of the *Nnat* gene display defective glucose-stimulated insulin secretion

To explore the role of *Nnat* in whole body metabolism, we generated mice with a global deletion of the *Nnat* gene (Figure 1A). A floxed *Nnat* allele ($Nnat^{flox}$) was first created in ES cells by the introduction of *lox*P sites flanking exon 1. A global *Nnat* null mouse line ($Nnat^{+/-}$) was then established following permanent excision of the flanked region by crossing $Nnat^{+/flox}$ mice with germline *Cre* recombinase expressing deleter mice. Global null $Nnat^{-/-}$ animals backcrossed onto the C57BL/6J strain background were viable and fertile and were born with a normal Mendelian ratio with normal litter sizes. In adult mice, neuronatin is primarily expressed in adipose tissue, hypothalamus, pituitary and pancreatic islet cells and RT-PCR and Western blotting analysis confirmed the absence of neuronatin expression in tissues of homozygous neuronatin knockout ($Nnat^{-/-}$) mice (Figure 1B, C). Heterozygous mice receiving the mutant allele from the paternal side ($Nnat^{+/-p}$) had undetectable levels of expression in islets, hypothalamus and white adipose tissue (WAT) at the mRNA and protein level, indicating that the imprinting status of *Nnat* was maintained in the mutant animals. In contrast, heterozygous mice receiving the mutant allele from the maternal side ($Nnat^{+/-m}$) displayed wild type levels of *Nnat* expression (Figure 1B, C). Targeting of *Nnat* did not affect expression of the biallelic gene *Blcap* found at the same locus (Supplemental Figure 1A).

In view of the existing evidence for a role for *Nnat* in energy homeostasis regulation we assessed body weight, feeding behavior (both *ad libitum* and after fasting) and in response to exogenous leptin. However, these were all unaltered in $Nnat^{+/-p}$ mice

compared to their wild type littermates (Supplemental Figure 1B-E). In contrast, when we analysed glucose homeostasis we found that *Nnat*$^{+/-p}$ mice displayed a profound defect in GSIS *in vivo* compared to wild type littermates, with complete absence of a response from basal insulin levels, as well as an unexpected basal hyperinsulinaemia (Figure 1D). This GSIS abnormality, which resulted in the loss of both phases of classical biphasic insulin secretion, was present in male knockout mice on both C57BL/6J and 129S2/Sv backgrounds (Figure 1D, Supplemental Figure 1F, plus insets).

To determine whether the perturbed GSIS seen in global *Nnat*$^{+/-p}$ mice was due to a beta cell-intrinsic defect, and because islet neuronatin expression is almost exclusively restricted to beta cells (Supplemental Figure 1G), we generated a beta cell-specific knockout line by crossing our *Nnat*^{flox} (floxed) line with mice harbouring *Cre* recombinase knocked in at the *Ins1* locus. This deleter strain catalyses efficient (~95%) recombination highly selectively in the beta cell, with undetectable activity at extrapancreatic sites (22, 23). RT-PCR and Western blotting confirmed loss of *Nnat* expression specifically in pancreatic islets of heterozygous mice with a floxed *Nnat* allele from the paternal side (βcellKO-*Nnat*$^{+/-p}$) but not from the maternal allele (βcellKO-*Nnat*$^{+/-m}$) and with no alterations in *Blcap* expression (Supplemental Figure 1H-J). While wild type, *Cre* positive, floxed, and βcellKO-*Nnat*$^{+/-m}$ mice all had normal GSIS (and were combined as controls) this was essentially abolished in βcellKO-*Nnat*$^{+/-p}$ mice (Figure 1E), indicating that the GSIS phenotype is beta cell autonomous. Glucose tolerance, although unaffected by *Nnat* deletion in chow-fed mice (Supplemental Figure 1K), was impaired in βcellKO-*Nnat*$^{+/-p}$ mice fed a Western diet for 4 weeks (Figure 1F), at which stage no differences in body weight or insulin

sensitivity were apparent between groups (Supplemental Figure 1L, M). These findings were also supported by *in vitro* studies using islets isolated from both global *Nnat*$^{+/-p}$ and conditional βcellKO-*Nnat*$^{+/-p}$ mice on a C57BL/6J background, which revealed a marked impairment in GSIS in the mutant beta cells (Global KO: 4.8-fold insulin secretion increase with high glucose in wild type vs 2.0-fold in *Nnat*$^{+/-p}$, n = 12, p = 0.0401; beta cell conditional KO: 7.2-fold increase in controls vs 4.2-fold in βcellKO-*Nnat*$^{+/-p}$, n = 8, p = 0.0207, Figure 2A and Figure 2B respectively). Taken together these findings indicate that *in vivo, Nnat* regulates beta cell function but has a limited effect on body weight and feeding behaviour.

Nnat deficient primary beta cells have a severe defect in insulin storage

Next, we explored a number of cellular and molecular mechanisms potentially responsible for defective GSIS in *Nnat* mutant animals. Impairment of GSIS was not due to a reduction in beta cell mass or disruption of islet architecture (Supplemental Figure 2A, B). The expression of key markers of the mature beta cell, including *Glut2 (Slc2a2)*, *Neurod1*, *Ins2*, *Pdx1* and *Nkx6.1* were all unaltered in islets from global *Nnat* knockout animals as were serum glucagon levels (Supplemental Figure 2C, D).

Manipulating expression of NNAT in beta cells and other cell types has previously been demonstrated to perturb intracellular Ca^{2+} homeostasis and dynamics and it has been suggested that this underlies the defect in GSIS found with *in vitro* knockdown of *Nnat* (5, 14, 20). In contrast, we obtained no evidence for altered Ca^{2+} signalling in islets from *Nnat*$^{+/-p}$ mice in response to either Ca^{2+} influx provoked by high glucose, or release of Ca^{2+} from intracellular stores in response to the activation of muscarinic

stimulation of Gq-coupled receptors, and the opening of ER resident inositol (1, 4, 5)-*tris*phosphate receptors (Supplemental Figure 2E).

To determine whether defective GSIS in *Nnat* deficient mice was due to a shortage of available cellular insulin, we measured mature insulin content in mutant primary islets by ELISA and found that this was considerably reduced compared to wild type islets, potentially indicating a defect in insulin storage (Figure 2C). We also found a similar reduction of proinsulin content in islets from mutant mice, resulting in an unaltered proinsulin to mature insulin ratio (Figure 2D, E). When primary islets from *Nnat*$^{+/-p}$ mice were treated with the proteasome inhibitor MG132 to prevent degradation of insulin precursors, Western blotting of lysates confirmed reduced mature insulin content in islets from mutant mice, and also the accumulation of unprocessed preproinsulin (Figure 2F). In contrast, no reduction in expression was observed for two other, ER membrane, proteins ribophorin I and IRE1alpha (Figure 2F). The defect in insulin storage was confirmed by transmission electron microscopy, with *Nnat*$^{+/-p}$ beta cells showing a striking lack of mature insulin-containing dense core secretory granules (DCSG), with an increased proportion of partially filled, or even "empty" (electron translucent) granules (Figure 3A-C). Together, these observations suggest a key *in vivo* role for *Nnat* in maintaining sufficient insulin content in pancreatic beta cells available for GSIS.

Neuronatin interacts with the signal peptidase complex

To gain further insights into the molecular roles of neuronatin and provide potential mechanisms for our *in vivo* observations, we employed an unbiased affinity purification mass spectrometry (AP-MS) screen with the aim of identifying novel

interaction partners of NNAT. We chose to focus on clonal pancreatic beta cells in our proteomic approach to avoid issues of cellular heterogeneity from whole pancreatic islets. Protein lysates from MIN6 cells, a mouse insulinoma-derived beta cell line (24), were incubated with antibodies against endogenous NNAT and the immunoprecipitate (IP) analysed by mass spectrometry (Figure 4A, Supplemental Figure 3A). Proteins co-immunoprecipitating with NNAT were ranked according to their abundance compared to control immunoprecipitates. Strikingly, of the top ranking proteins in this analysis, three were components of the signal peptidase complex (SPC), namely the catalytic subunit SEC11A and signal peptidase complex subunits 1 and 2 (SPCS1 and 2, Figure 4B, Supplemental Table 1 for full list), a complex responsible for cleavage of the signal peptide (SP) from nascent preprohormones. To verify the interaction between NNAT and the SPC, tagged versions of SEC11A and NNAT were expressed in cultured cells. FLAG-tagged NNAT co-immunoprecipitated with c-Myc tagged SEC11A, confirming the association between NNAT and the SPC (Figure 4C).

Neuronatin enhances signal peptidase activity *in vitro*

The role of the SPC in the SP cleavage of preproinsulin has, in part, been established through the identification of human *insulin* gene mutations that alter preprohormone processing. This in turn impairs beta cell function leading to a spectrum of diabetic phenotypes (25, 26). SiRNA-mediated transient silencing of *Sec11a* in the INS1E beta cell line (27) reduced both insulin content and secretion in high glucose conditions (Figure 4D, Supplemental Figure 3B, C) suggesting a key role of the SPC in insulin maturation and subsequent release. Likewise, knockdown of *Nnat* caused a reduction

in insulin content and marked blunting of GSIS (Figure 4D, Supplemental Figure 3B, C).

To determine whether there is a direct role for NNAT in preproinsulin SP cleavage, we followed this event in newly synthesised preprohormone by pulse-labelling with ^{35}S-Met/Cys. In scramble siRNA control-transfected cells, preproinsulin was rapidly processed to proinsulin and subsequently secreted (Figure 4E, F). In contrast, *Nnat* silencing reduced preproinsulin SP cleavage, with significant preproinsulin accumulation (Figure 4E). Following a 3-hour chase period we observed reduced secretion of proinsulin as well as some intracellular proinsulin loss, presumably reflecting degradation (Figure 4F). An even more marked defect in SP cleavage and secretion was observed upon knockdown of *Sec11a* (Figure 4E, F). Together, these data suggest that NNAT interacts with, and modulates, preproinsulin processing by the SPC.

NNAT resides on the cytosolic face of the ER membrane to regulate preproinsulin translocation

To explore the possibility of a direct effect of NNAT on signal peptidase activity we used an *in vitro* translation system in which preproinsulin was synthesised in the presence of pancreatic microsomes, ER membrane fragments containing endogenous signal peptidase (and glycosylation) activity (28, 29). Initially, we confirmed that the microsomal membranes were able to support proteolytic cleavage of c-Myc tagged preproinsulin, yielding an 11 kDa fragment corresponding to SP-cleaved proinsulin (Supplemental Figure 4A). Translation assays involving co-expression of c-Myc tagged preproinsulin and either FLAG-tagged NNAT or GFP were then performed,

with each reaction including a fixed concentration of microsomal membranes as a source of SPC. This approach demonstrated that co-expression of NNAT caused a small but significant augmentation of the SP processing of newly synthesised preproinsulin (Figure 5A), and suggest a key contribution for NNAT in the efficient functioning of the SPC.

Improper processing of preproinsulin might reflect reduced enzymatic activity of the SPC and/or failure of efficient preproprotein translocation across the ER membrane to the luminal surface where catalytic activity resides. To dissect the potential contribution of NNAT to each process, we first investigated whether preproinsulin targeting to the ER was perturbed in the absence of NNAT. Clonal INS1E beta cells silenced for *Nnat* by RNAi were radiolabelled as above and treated with digitonin to specifically permeabilise plasma membranes, leaving internal (ER, secretory granule) membranes intact. Treatment of cells with digitonin, and subsequent centrifugation, led to a shift of GAPDH from the pellet to the supernatant, whereas insulin precursors were retained in the pellet in both control and *Nnat* silenced cells. Thus, association of nascent preproinsulin with the ER is not perturbed upon silencing of NNAT (Figure 5B). This observation indicates that, in the absence of NNAT, preproinsulin is still efficiently targeted to the ER membrane. However, it does not exclude the possibility that preproinsulin is not fully translocated across the ER membrane. To test this, we examined endogenous preproinsulin distribution by immunofluorescence in digitonin treated, and thus partially permeabilized cells, using an antibody that detects both preproinsulin and mature insulin. Preproinsulin staining in digitonin treated cells was only detected upon RNAi silencing of NNAT, suggesting that the preproinsulin moiety was untranslocated and exposed to the cytosol, whereas in control cells this

was virtually absent indicating complete translocation into the ER (Figure 5C). The ER luminal protein protein disulfide isomerase (PDI), which was used to monitor permeabilisation, was only stained after disruption of all membranes using Triton X-100 (Figure 5C). Together, these data demonstrate that, in the absence of NNAT, preproinsulin is still targeted to the ER but exhibits impaired translocation across the ER membrane.

Three of the five SPC subunits reside on the luminal side of the ER membrane (SEC11A, SEC11C, SPCS3), including both catalytic subunits, with the bulk of the remaining two proteins lying on the cytosolic side (SPCS1 and 2) (30, 31). NNAT is a membrane-resident protein (Supplemental Figure 4B), with a proposed transmembrane region at the N-terminus. However, the localisation of the C-terminal region has not been determined. To interrogate the topology of the SPC interaction with NNAT, we used *in vitro* translation to express C-terminally-tagged NNAT on microsomal membranes and assessed susceptibility to proteinase K treatment. C-terminally-tagged SPCS3 and SEC11A, a region of each protein known to be luminal (31) and therefore on the inside of the microsome, were used as controls. NNAT translation in the presence of microsomes did not alter its molecular weight suggesting that NNAT itself is not cleaved or glycosylated (Figure 5D). Levels of the glycosylated form of SPCS3, represented by the upper band in Figure 5D, was increased in the presence of microsomes (31). Although the amount of SPCS3 and SEC11A protein was not altered by proteinase K treatment, presumably reflecting sequestration within microsomes, NNAT protein levels were substantially reduced in the presence of the protease indicating that its C-terminal region and indeed the bulk of this protein is located on the cytosolic side of the ER membrane (Figure 5D). We

further verified this observation in clonal INS1E beta cells by fixing and permeabilising cells with digitonin and immunostaining for endogenous NNAT with an antibody that recognises the C-terminal domain. Digitonin treatment was sufficient to allow staining of NNAT, but not PDI, which was only stained after permeabilisation of all membranes using Triton X-100 (Figure 5E). Together, these experiments demonstrate that the bulk of the NNAT protein and its C terminus is located on the cytosolic side of the ER membrane, with an N-terminal anchor sequence (Figure 5F).

Depletion of NNAT delays proinsulin exit from the ER

In our mass spectrometry analysis NNAT also co-immunoprecipitated with a number of Coat protein complex II-associated (COPII; namely SEC31A, SEC13, p115) and microtubular (gamma-tubulins) proteins (Figure 4B, Supplemental Table 1). We therefore asked whether these interactions were of functional significance. COPII-coated vesicles mediate the exit of cargo proteins from the ER, with membrane budding occurring at discrete locations on the ER known as ER exit sites. Vesicles then travel towards a vesicular-tubular cluster of membranes known as the ER-Golgi intermediate compartment (32, 33) (ERGIC) raising the possibility that NNAT is required for efficient proinsulin exit from the ER. Using cycloheximide to block new proinsulin synthesis and monitor existing proinsulin decrease as molecules mature through the secretory pathway, we demonstrate in NNAT-silenced INS1E that proinsulin levels were significantly higher in knockdown cells, consistent with slower dynamics of proinsulin exit from the ER (Figure 6A). Immunofluorescent staining of subcellular markers in INS1E indicated that NNAT was present throughout the ER (as labelled with PDI staining) and in the ERGIC compartment (ERGIC53) but did not

itself migrate to the *cis*-Golgi face (*cis*-Golgi matrix of 130 kDa, GM130) or *trans*-Golgi network (TGN38) (Figure 6B). Overall, it appears that NNAT is required for efficient SP processing and maturation of preproinsulin through the early secretory pathway in the ER.

Nnat expression is glucose-sensitive in rodent beta cells

We (11, 15), and others (12, 13), have previously shown that *Nnat* expression is responsive to nutritional status in adipose tissue and hypothalamus. In view of the important role of NNAT in insulin SP cleavage and GSIS (Figure 1-5), we further examined the regulation of *Nnat* expression by glucose. In the present studies, acute (6-hour) incubation of isolated mouse islets (Figure 6C, D) or clonal INS1E beta cells (Supplemental Figure 5A) with high (16.7 mM) glucose caused rapid up-regulation of *Nnat* mRNA and protein. Fasting in mice resulted in reduced NNAT protein levels in pancreatic islet cells while acute high fat feeding led to higher levels (Figure 6E). Changes with similar dynamics were observed in adipose tissue (Supplemental Figure 5B, C) and hypothalamus (Supplemental Figure 5D) from the same animals. Together, it appears that changes in the cellular levels of NNAT in response to nutritional cues, notably glucose, co-ordinately regulate subsequent alterations in demand for insulin SP cleavage by fluctuating glucose levels.

Discussion

The present studies demonstrate a key and novel role for the nutrient-sensitive, imprinted gene neuronatin in the regulation of pancreatic beta cell function. Through a series of *in vitro* and *in vivo* approaches, we show that NNAT directly interacts with the SPC to regulate the efficiency of preproinsulin signal peptidase cleavage. Neuronatin expression itself is glucose-regulated, thus revealing a previously unrecognized point of metabolic control for early insulin maturation and therefore its storage and secretion. Loss of neuronatin function thus results in a profound defect in GSIS both *in vitro* and in the living animal.

The majority of secreted proteins are synthesised with an amino-terminal SP, directing them into the secretory pathway via the ER. Here, the membrane-bound SPC cleaves the SP, an essential step in the maturation and eventual secretion of the mature protein (34, 35). In mammals, the SPC consists of five subunits: SEC11A and SEC11C which are responsible for the catalytic activity and are present in the ER lumen (31, 36, 37) and SPCS1, 2 and 3. SPCS1 and 2, which are found on the cytosolic face, appear to affect proteolytic efficiency without possessing intrinsic catalytic activity, possibly by mediating preproprotein translocation across the ER membrane (30, 38-41). We show that, in pancreatic beta cells, NNAT is located on the cytosolic face of the ER, presumably interacting with SPCS1 and 2 where it promotes translocation but not targeting of nascent proinsulin into the ER. In contrast, we obtained little evidence for localization to the plasma membrane as suggested by others (21).

Our loss of function studies demonstrate that NNAT is required for efficient SP cleavage of preproinsulin by the SPC in beta cells. Thus, disruption of this step results in reduced intracellular proinsulin and would appear to therefore lead to a profound defect in mature insulin storage and secretion, with mice lacking *Nnat* either globally or specifically in beta cells displaying severely impaired GSIS. Interestingly, we have been unable to find previous published evidence to suggest that this early stage of insulin processing by the SPC is subject to specific regulation and consequently, it has been assumed that this step is constitutive in nature. Our RNAi studies in the INS1E beta cell line demonstrate the importance of adequate SPC activity for insulin maturation and that early defects are able to propagate through the system and result in blunted GSIS. Furthermore, a key role for appropriate cleavage of the insulin SP in normal glucose homeostasis has previously been revealed by the identification of rare human genetic mutations within the SP region of preproinsulin (26). These mutations disrupt SP cleavage leading to reduced insulin secretion in a dominant fashion, resulting in ER stress and beta cell apoptosis, in a form of diabetes termed mutant insulin gene-induced diabetes of youth (MIDY) (25, 26, 42, 43). The magnitude of this beta cell stress from mutant insulin species dictates the outcome of severe/early onset or mild/late onset diabetes. For example, an R6C mutation causes a ~50% reduction in translocation into the ER, with untranslocated molecules degraded in the cytosol. Successfully translocated preproinsulin is efficiently processed and secreted, with no evidence for ER stress, resulting in a milder form of mid to late onset diabetes (42, 44, 45). In contrast, an A24D insulin mutation does not affect preproinsulin translocation but completely blocks SP cleavage by SPC in the ER lumen, leading to misfolding and accumulation of unprocessed preproinsulin and subsequent ER stress, beta cell failure and neonatal diabetes (43, 46). We did not observe any evidence of

ER stress in islets after *Nnat* inactivation *in vivo* (data not shown) with *in vitro* studies indicating a defect in preproprotein translocation on the cytosolic side of the ER membrane, where the bulk of the NNAT protein resides. Pulse chase and immunofluorescence analysis further suggested that untranslocated preproinsulin is degraded in the cytosol. Consistent with this lack of ER stress, the proinsulin to mature insulin ratio in mutant islets was unaltered, indicating that processing of the C-peptide, downstream of the SP processing event cleavage and mediated by prohormone convertases (PCSK1 and PCSK2) and carboxypeptidase E (CPE), was unaffected. It is therefore clear that loss of neuronatin does not cause an absolute block in preproinsulin SP cleavage, as can occur in severe forms of MIDY. This may explain the lack of development of progressive diabetes in *Nnat* deficient mice despite the presence of a severe defect in GSIS and glucose intolerance under nutrient overload, due to the absence of ER stress and subsequent beta cell failure that can result from the accumulation of mis-folded insulin species.

Instead, beta cell *Nnat* deficiency in mice causes loss of appropriate insulin secretion control, with complete absence of glucose-evoked insulin release and glucose intolerance under conditions of dietary excess. The mildly increased basal insulin secretion observed *in vivo*, but not in primary islets likely stems from compensatory responses from lack of GSIS during periods of increased demand i.e. feeding, and is perhaps the reason for the lack of any glucose intolerance found in chow fed mice. We also observe that NNAT expression in beta cells is rapidly responsive to acute changes in nutrient conditions both *in vitro* and *in vivo*.

Our studies also provide important insights into the previously preposed mechanisms through which neuronatin regulates cell physiology. Over-expression studies *in vitro* in both beta cell and adipocyte cell lines had suggested that neuronatin regulates intracellular calcium handling (5, 14). In contrast, the present detailed studies of Ca^{2+} dynamics in *Nnat* null primary beta cells failed to reveal any defects. These findings strongly suggest that neuronatin is unlikely to be involved in shaping Ca^{2+} signals in these cells and specifically in the proximal calcium-dependent events underpining glucose-sensing (47). Furthermore, it does not appear that NNAT is present on insulin secretory granules itself. The ER localisation of NNAT and its binding partners documented in this work regulating SP cleavage, and our subsequent experiments in these early events points to a major role during initial peptide handling rather than other events involved in GSIS.

Previous studies have also indicated that neuronatin may play a role in the central nervous system regulation of metabolism, and in particular body weight, as its expression in specific hypothalamic regions is regulated by leptin and nutrients (12, 13). Furthermore, rare single nucleotide polymorphisms at the human *NNAT* locus are associated with extreme childhood obesity (17). The lack of marked body weight, feeding or energy expenditure phenotypes in *Nnat* null mice, plus preserved sensitivity to exogenous leptin, suggest that neuronatin does not play a major role in these aspects of energy metabolism.

In summary, we demonstrate an unexpected role for neuronatin in the control of early preproinsulin SP cleavage, which leads to marked deficits in insulin storage and secretion thus defining a previously unrecognized site of nutrient-sensitive control of

beta cell function and whole animal glucose homeostasis. Importantly, the requirement for neuronatin in SP cleavage, and the expression of this protein in a range of neuronal, adipose and endocrine cell types involved in the regulation of metabolism and growth, suggests additional roles in neuroendocrine cell secretion and the regulation of energy homeostasis. Future studies will be required to explore these possibilities.

Methods

Reagents

Mouse monoclonal antibodies against insulin (Clone K36AC10, I2018, for immunostaining of paraffin sections), FLAG (M2, F1804), β-tubulin (DM1A, T9026) and glucagon (K79bB10, G2654) were from Sigma-Aldrich. Rabbit polyclonal antibodies against glucagon (ab92517), NNAT (ab27266), VAPB (ab72470), TMED9 (ab97651), ribophorin I (ab198508) and mouse monoclonal antibodies against PDI (RL90, ab2792) were from Abcam. Mouse anti-insulin (L6B10, 8138, for immunoblotting/immunofluorescence), anti-Myc (9B11, 2276) and anti-IRE1alpha (14C10, 3294) were purchased from Cell Signalling. Mouse monoclonal antibodies against ERGIC53 (G1/93, ALX804602), TGN38 (2F7.1, MA3-063) and GM130 (35/GM130, 610822) were from Enzo Life Sciences, Thermo Fisher and BD Biosciences, respectively. MG132 and cycloheximide were purchased from Sigma-Aldrich.

Animal models

Experiments involving animals were designed and reported following the ARRIVE guidelines of animal experiment reporting. Power calculations for number of mice for each experiment were based on reported or known effect sizes and variation, in order to maximise chances of meaningful results without the unnecessary use of experimental animals. Where possible, investigators were blinded to the genotype of both study animals and tissue/blood samples. For experiments involving treatments, mice were randomised by genotype for study groups, or a crossover design was used where indicated. All metabolic studies were replicated in at least two independent

cohorts and key *in vivo* findings were confirmed in mice of both sexes.

A floxed *Nnat* allele was created by homologous recombination in ES cells. *Lox*P sites were introduced flanking exon 1 of the *Nnat* gene, with a *neomycin* cassette flanked by FRT sites used as a selectable marker (GenOway, France). 129S2/SvPas ES cells were transfected with linearised targeting vector JSC1-HR by electroporation, and DNA from clones screened by Southern blotting and PCR. ES cells were injected into blastocysts, which were implanted into pseudopregnant females and chimeric male mice screened for germline transmission. Flp-mediated excision to delete the *neomycin* selection cassette (Neo) was performed *in vivo* by breeding mutant animals with ubiquitous *Flp* recombinase expressing deleter mice, to produce a floxed *Nnat* allele ($Nnat^{+/flox}$). Mice with constituent deletion of *Nnat* were then created by intercrossing the $Nnat^{+/flox}$ line with a *Cre* recombinase expressing deleter strain in order to generate a null version of this allele ($Nnat^{+/-}$). Both of these mouse lines were backcrossed in our transgenic animal facility >8 times onto C57BL/6J or 129S2/Sv backgrounds before intercrossing of mutant animals for generation of experimental cohorts. The presence of the mutant allele was determined by PCR analysis of DNA from ear tissue biopsies. A common upstream primer (5'-TGGTCTACTTCTCCATAAAGCTCGCTCC-3') and primers specific for the wild type allele (5'-GATCTTTTCTGACTGTTGGTTCCCGC-3') and a region downstream of the excised sequence (5'-AAGGGGCATTTTTTTCTCTAGTGTGTTTCC-3') were used for amplification.

To delete *Nnat* specifically in pancreatic beta cells, $Nnat^{+/flox}$ mice were crossed with transgenic mice expressing *Cre* recombinase at the *Ins1* locus (23) to generate mice with conditional deletion of *Nnat* in beta cells.

Experimental cohorts of group housed, young adult mutant male mice and their control littermates were maintained on a 12-hour light/dark cycle with free access to water and standard mouse chow (RM3, Special Diet Services) and housed in specific pathogen-free barrier facilities. All animal work was carried out in accordance with the UK Animals (Scientific Procedures) Act (1986). High fat diet (D12451, 45% energy from fat, 35% energy from carbohydrate) and high sugar/high fat Western cafeteria diet (D12079B, 40% energy from fat, 43% energy from carbohydrate) were both purchased from Research Diets.

Metabolic analysis

Measurement of body weights, tail vein blood collection and determination of blood glucose levels using a Contour glucometer (Bayer) were all performed as previously described (48). Intraperitoneal glucose (2 g/kg) and insulin (0.75 IU/kg) tolerance tests as well as intraperitoneal GSIS (3 g/kg) were all performed as (49) with blood collection at times indicated in the figure. Assessment of food intake and leptin sensitivity was performed in singly housed mice for 3 consecutive experimental days as previously described (48) using 1.5 mg/kg recombinant mouse leptin (R&D Systems). Levels of mature insulin (no cross reactivity with proinsulins) and both proinsulin and glucagon were determined by ELISA (Crystal Chem and Mercodia respectively).

Primary islet isolation and GSIS

For islet isolation, the pancreas was injected with Liberase TM (Roche), digested at 37°C, purified using a Histopaque gradient (Sigma-Aldrich) and handpicked as previously described (50). For secretion studies, isolated islets were cultured

overnight in RPMI supplemented with 10% FBS. Following a 30 minute pre-incubation in Krebs-HEPES-Bicarbonate buffer (KHB, 140 mM NaCl, 3.6 mM KCl, 0.5 mM NaH_2PO_4, 0.2 mM $MgSO_4$, 1.5 mM $CaCl_2$, 10 mM HEPES, 25 mM $NaHCO_3$) with 3 mM glucose, GSIS was assessed by static incubation of six sized matched islets in KHB with 3 mM or 16.7 mM glucose for 30 minutes at 37°C. Secreted mature insulin into the media and total mature insulin content of the islets was assayed by ELISA (Crystal Chem, no cross reactivity with proinsulins).

Calcium imaging

Calcium imaging was performed in KHB buffer saturated with 95% O_2/5% CO_2 and adjusted to pH 7.4, with additions as stated in the figures. Islets were incubated at 37°C for 45 minutes in KHB buffer containing 10 μM Fluo-2-AM (Cambridge Biosciences). Islets were then transferred in a perfusion chamber, mounted on a Zeiss Axiovert confocal microscope and continuously perfused at 34-36 °C. Fluo-2 was excited with a 491 nm laser line and emitted light filtered at 525/50 nm. Images were acquired with a Hamamatsu ImagEM camera and Volocity software (Perkin Elmer) was used for data capture. Traces are presented as normalised intensity over time (F / F0) (51).

Transmission electron microscopy (TEM)

Isolated islets were fixed in 4% PFA/0.2% glutaraldehyde in PBS at 4ºC overnight immediately upon extraction. Samples were washed three times with cacodylate buffer (Electron Microscopy Sciences, EMS) and osmicated with osmium tetroxide in 2% (w/v) cacodilate buffer for 1 hour. Samples were then washed five times with deionized water and dehydrated through a graded ethanol series. After dehydration,

samples were infiltrated with Epon Resin (EMS) diluted in ethanol at 3:1, 2:1, and 1:1 for 1 hour each, and then overnight at 1:2. The solution was then replaced with pure resin, which was changed twice in the first 12 hours and then allowed to infiltrate again overnight. Samples were immediately placed in an oven at 60°C and left to cure overnight. Curetted resin blocks were sectioned at 100 nm using an ultramicrotome (Leica) and immediately placed on copper grids. These grids were imaged in a TEM at 80 kV (JEOL 2000FX TEM).

Histological techniques and Immunofluoresence

Dissected pancreases were fixed in Bouin's solution, embedded in paraffin and cut into 5 μm sections. Insulin (mouse monoclonal, Sigma-Aldrich) and glucagon (rabbit polyclonal, Abcam) immunostaining, and morphometric analysis were performed blindly as previously described using a DMRB Fluorescence microscope (Leica) (48). Dispersed islets and INS1E grown overnight on poly-L-lysine coverslips were fixed in 4% PFA, permeabilised, and immunostained with primary (listed in reagents section) and secondary antibodies (Alexa Fluor-488 and -594, Invitrogen). Cells were mounted on glass slides and imaged using a TCS SP5 II Confocal microscope (Leica).

Immunoprecipitation and Mass Spectrometry

MIN6 cells (24) grown in standard culture conditions (DMEM, 10% FBS, 2 mM L-Glutamine, 50 μM beta-mercaptoethanol, 37ºC, 5% CO_2) were homogenised in protein lysis buffer (50 mM Tris-HCl pH 7.5, 150 mM NaCl, 1% Triton X-100, 1 mM EDTA with protease inhibitors (Complete mini from Roche)), clarified and normalised for protein content. Supernatants were incubated with protein A-agarose beads (Calbiochem) and antibodies against NNAT (rabbit polyclonal, Abcam) or

rabbit IgG (control IP) rotating at 4ºC overnight. Beads were washed four times with lysis buffer, boiled in Laemmli buffer, run on SDS-PAGE and gels stained with Coomassie (SimplyBlue, Invitrogen). Each lane was excised into bands and placed into separate protein lo-bind Eppendorf tubes for proteomic analysis by mass spectrometry. Coomassie was removed from bands by incubation with 50 mM ammonium bicarbonate, 10% acetonitrile for 30 minutes at room temperature and gel pieces dehydrated for 10 minutes. Disulfide bonds were reduced using 10 mM dithiothreitol and free thiol groups alkylated with 55 mM iodoacetamide. Modified porcine trypsin (Proteomics Grade, Sigma-Aldrich) was added to each gel piece to a final amount of 0.5 µg and incubated overnight at 37ºC, with tryptic digestion halted by addition of 5% formic acid. Peptide-containing solutions were dried in a vacuum centrifuge, before peptides were solubilised in 30 µL of 0.1% trifluoroacetic (TFA) and placed in autosampler vials ready for LC-MS injection.

Peptides were separated using an Ultimate 3000 nano liquid chromatography system (Thermo Scientific) prior to mass spectrometric analysis. 5 µL of sample was loaded onto a trap column (Acclaim Pepmap 100, 100 µm × 2 cm, C18) at 8 µL/min in 2% acetonitrile, 0.1% TFA. Peptides were then eluted on-line to an analytical column (Acclaim Pepmap RSLC, 75 µm × 25 cm, C18) and separated using a ramped gradient. Eluted peptides were analysed by a LTQ Velos Orbitrap mass spectrometer operating in positive polarity data-dependent acquisition mode. Ions for dissociation were determined from an initial 15000-resolution MS survey scan (event 1) followed by CID (collision-induced dissociation) of the top 10 most abundant ions (500 count threshold). CID conditions were default charge state 2, 2.0 m/z isolation width, normalised collision energy 35.0, Activation Q value 0.25, activation time 10 ms, lock

mass value of 445.120030 m/z. Progenesis QI for Proteomics (Waters Corp, USA) software was used to align all raw data files, perform peak picking and produce features for export as mgf files. Mascot and Mascot Daemon v2.5.1 (Matrix Science, UK) were used to search mgf files against the Swissprot *Mus musculus* database (downloaded 2014.11.26 containing 16,686 sequences). A reversed decoy was implemented by Mascot and results were filtered to 1% false discovery rate. Search parameters included: 10 ppm MS1 tolerance, 600 mmu MS2 tolerance, maximum of 2 missed cleavages, fixed modification of cysteine carbamidomethylation and variable modifications of methionine oxidation and protein N-terminal acetylation. Resulting XMLs were returned to Progenesis and proteins filtered for those containing at least one unique peptide and identified in all three biological replicates. Intensity normalisation was performed by Progenesis, and proteins were ranked by fold change increase in abundance compared to control IPs.

For validation experiments in HEK293T (cultured in DMEM, 10% FBS, 2 mM L-Glutamine, 37ºC, 5% CO_2) cells were transfected with plasmids expressing C-terminal c-Myc tagged SEC11A (Origene) and C-terminal FLAG-tagged mouse NNAT in pcDNA3.1 (BamHI/XhoI sites) using Lipofectamine 2000. 48 hours later, transfected cells were lysed, clarified, normalized as above and immunoprecipitated using anti-c-Myc agarose resin (Pierce) with Western blotting performed using antibodies against c-Myc (mouse monoclonal, Cell Signalling) and FLAG (mouse monoclonal, Sigma-Aldrich).

INS1E siRNA knockdown

For siRNA silencing, INS1E cells (52) (cultured in RPMI, 10% FBS, 2 mM L-

Glutamine, 50 μM beta-mercaptoethanol, 37ºC, 5% CO_2) were transfected with 50 nM of Silencer Select siRNAs (*Nnat*: s137247 and *Sec11a*: s80747, both Ambion) using Dharmafect 1 reagent (Dharmacon). After 24 hours, cells were incubated overnight in cell culture medium with 3 mM glucose. For GSIS the following day, cells were incubated for 30 minutes in KHB with 3 mM glucose at 37ºC and then with 3 mM glucose or 25 mM glucose for a further 30 minutes at 37ºC. Secreted insulin into the media and total cellular insulin content were assayed by ELISA (Crystal Chem). For cycloheximide chase assay, INS1E with siRNA-mediated knockdown were treated with 15 μg/ml cycloheximide (Sigma-Aldrich) for 2 hours prior to homogenisation in protein lysis buffer as above and proteins analysed by Western blotting.

Pulse chase analysis

Radiolabelling was performed in INS1E cells with transient transfection of C-terminal c-Myc tagged mouse preproinsulin II (Origene) and siRNAs. 48 hours post transfection, cells were pulse-labelled with ^{35}S-methionine/cysteine (Perkin Elmer) for 15 minutes and chased with unlabelled media where indicated, essentially as described in (42, 43). Cells were homogenised in protein lysis buffer as above and centrifuged at 16,000 x g for 10 minutes at 4ºC. Cell lysates and chase media were immunoprecipitated using c-Myc agarose resin (Pierce), and analysed by SDS-PAGE and standard autoradiography techniques including enhancement with Amplify reagent (GE Healthcare).

ER targeting assay

For assessment of preproprotein targeting to the ER, INS1E cells were transfected

with preproinsulin II and siRNAs as above with the inclusion of a vector expressing c-Myc tagged mouse GAPDH (Origene) and radiolabelled for 15 minutes. Cells were then washed and resuspended in 50 μL of 50 mM HEPES, 150 mM NaCl, 2 mM $CaCl_2$, pH 7.5 with protease inhibitors +/- 0.01% digitonin for 10 minutes on ice. Cells were centrifuged at 16,000 x g for 10 minutes at 4ºC, after which 450 μL of protein lysis buffer (1% Triton X-100, as above) was transferred to the supernatant, and the pellet lysed in 500 μL protein lysis buffer. Both supernatant and pellet were immunoprecipiated with c-Myc agarose resin and analysed by autoradioagraphy as above, all as described previously (42, 43), and with 3 independent experiments performed.

Assays in partially permeabilised cells

For membrane orientation of NNAT in INS1E, cells grown on poly-L-lysine coverslips were fixed with 4% PFA, permeabilised with either 0.01% digitonin or Triton X-100 and immunostained with antibodies against NNAT (rabbit polyclonal, Abcam) or PDI (mouse monoclonal, Abcam). Images were acquired using a TCS SP5 II Confocal microscope (Leica), all as (42). To assess preproinsulin translocation across the ER membrane, INS1E cells were grown on poly-L-lysine coverslips, with siRNA-mediated knockdown of *Nnat* for 48 hours. Cells were pretreated with MG132 for 4 hours prior to fixation, permeabilised with either digitonin or Triton X-100 as above and immunostaining was performed using antibodies against preproinsulin/mature insulin (Cell Signalling), NNAT and PDI. Both of these experiments were performed at least three times independently and representative images shown are maximum projections from 3-step Z-stacks 0.5 μm apart.

Cellular membrane preparation

INS1E cells were homogenised in a hypotonic buffer (50 mM Tris-HCl pH 7.5, 50 mM mannitol, 1 mM EDTA with protease inhibitors) and cleared by centrifugation at 1,000 x g for 10 minutes at 4ºC. The supernatant was layered upon a mannitol cushion (same buffer as above but 300 mM mannitol) and ultra-centrifuged (Optima TLX Ultracentrifuge, Beckman Coulter) at 60,000 x g for 60 minutes at 4ºC. Both the crude membrane pellet and the supernatant were resuspended in Laemmli buffer, boiled, and proteins analysed by Western blotting using antibodies against NNAT (rabbit polyclonal, Abcam), VAPB (rabbit polyclonal, Abcam), TMED9 (rabbit polyclonal, Abcam) and β-tubulin (mouse monoclonal, Sigma-Aldrich).

Expression analysis

Snap frozen tissues or cells were homogenised directly into Trizol reagent for RNA analysis or lysis buffer (50 mM Tris-HCl pH 7.5, 150 mM NaCl, 1% Triton X-100, 1 mM EDTA with protease inhibitors (Complete mini from Roche)) for protein work. mRNA was extracted using RNeasy kits (Qiagen), normalized for cDNA synthesis, and expression assessed by quantitative RT-PCR using Taqman reagents on a 7900HT Real Time PCR cycler (All Applied Biosystems). A complete list of probes used for quantitative RT-PCR is available in Supplemental Table 2. Protein expression was analysed by Western blotting from clarified lysates normalized for protein content by BCA method (Bio-Rad), all as previously described (48). A complete list of primary antibodies can be found in the reagents section.

Signal peptidase assay

Cell free cleavage of SP from preprohormones *in vitro* has been described previously (28, 29). Briefly, cDNAs for *preproinsulin*, subunit components of the SPC (*Sec11a* and *Spcs3*), all with a C-terminal c-Myc tag (purchased from Origene) as well as C-terminal FLAG tagged full length *Nnat* and untagged *Gfp* were PCR amplified and cloned into the MscI/SalI sites of the pT7CFE1.CHis vector. Stop codons were included after each tag to prevent expression of the endogenous His tag. Proteins were translated from these constructs *in vitro* using a human (HeLa based) *in vitro* translation kit (Pierce) by incubation at 30ºC for 90 minutes. Where indicated, canine pancreatic microsomes (Promega) were included in the reaction. A standard concentration of pancreatic microsomes was used per reaction as a source of SPC, which generated partial (~50%) processing of the total amount of preproinsulin, but allowed a significant proportion of unprocessed preproinsulin in order to determine augmenting effects of exogenous NNAT on these processing dynamics. Samples from 3 independent experiments were boiled in Laemmli buffer and abundance of proteins in these reactions determined using Western blotting with anti c-Myc and FLAG antibodies.

Nnat membrane topology

For orientation of NNAT on the microsomal membrane, 90 minute translations expressing NNAT, SPCS3 or SEC11A were adjusted to a final concentration of 2 mM $CaCl_2$, and +/- 10 μg/mL Proteinase K, +/- 1% Triton X-100 where indicated and transferred to ice for 30 minutes. Addition of Triton X-100 detergent to disrupt microsomes served as a positive control for proteinase K activity. Proteolysis was terminated by addition of PMSF, and samples from 3 independent experiments were

boiled in Laemmli buffer prior to analysis by Western blotting using antibodies against c-Myc and FLAG, essentially as (31).

Statistics

Statistical significance between groups was determined using GraphPad Prism 7 by two-tailed Student *t* test, Mann-Whitney U test or ANOVA, with Bonferroni post-hoc tests performed where appropriate. A probability of error less than 5% was considered significant (i.e., $p < 0.05$). Statistical information for experiments (data representation, *p* values and *n* numbers) can be found in the figure legends.

Study approval

All animal work was carried out in accordance with the UK Animals (Scientific Procedures) Act (1986).

Author Contributions

S.J.M., G.A.R., J.S. and D.J.W. designed the research; S.J.M., G.Da.S.X., A.I.C., S.B., P.C., S.M.A.P., E.E.I., A.M., P.F., J.K.-C., F.P. and M.L. performed experiments; W.R.T and J.F. contributed new reagents/analytical tools; S.J.M., R.M.J., M.L., M.L., G.A.R., J.S. and D.J.W. drafted and/or wrote the manuscript; M.C., G.A.R., J.S. and D.J.W. provided funding; G.A.R., J.S. and D.J.W. supervised the work.

Acknowledgements

We are grateful to Suchira Gallage, Darran Hardy, Justyna Glegola, Paulius Viskaitis, Matthew Gordon, Alex Sardini, Angela Woods, Naveenan Navaratnam, Dirk Dormann and Chad Whilding for technical help and advice with some experiments. This work was supported by a Wellcome Trust Project Grant (093082/Z/10/Z) to J.S., D.J.W. and M.C., a Wellcome Trust Strategic Award (098565/Z/12/Z) to D.J.W. and funding from the Medical Research Council (MC-A654-5QB40) to D.J.W. G.A.R. received grants from the Wellcome Trust (Senior Investigator Award WT098424AIA), Diabetes UK (Projects BDA/11/0004210, BDA/15/0005275), the MRC (UK; Programmes MR/J0003042/1, MR/L020149/1 "DIVA"; Project MR/N00275X/1) and a Royal Society Research Merit Award. GDaSX thanks Diabetes UK for Project grant BDA/13/0004672. W.R.T. was funded by The Francis Crick Institute (FC001179). Research in the M.L. laboratory was funded by research grants from National Natural Science Foundation of China (81070629, 81620108004 and 81370895).

References

1. Surani MA. Genomic imprinting: control of gene expression by epigenetic inheritance. *Curr Opin Cell Biol*. 1994;6(3):390-5.
2. Peters J. The role of genomic imprinting in biology and disease: an expanding view. *Nat Rev Genet*. 2014;15(8):517-30.
3. Dou D, and Joseph R. Cloning of human neuronatin gene and its localization to chromosome-20q 11.2-12: the deduced protein is a novel "proteolipid'. *Brain Res*. 1996;723(1-2):8-22.
4. Joseph R, Dou D, and Tsang W. Neuronatin mRNA: alternatively spliced forms of a novel brain-specific mammalian developmental gene. *Brain Res*. 1995;690(1):92-8.
5. Suh YH, Kim WH, Moon C, Hong YH, Eun SY, Lim JH, et al. Ectopic expression of Neuronatin potentiates adipogenesis through enhanced phosphorylation of cAMP-response element-binding protein in 3T3-L1 cells. *Biochem Biophys Res Commun*. 2005;337(2):481-9.
6. Evans HK, Wylie AA, Murphy SK, and Jirtle RL. The neuronatin gene resides in a "micro-imprinted" domain on human chromosome 20q11.2. *Genomics*. 2001;77(1-2):99-104.
7. John RM, Aparicio SA, Ainscough JF, Arney KL, Khosla S, Hawker K, et al. Imprinted expression of neuronatin from modified BAC transgenes reveals regulation by distinct and distant enhancers. *Dev Biol*. 2001;236(2):387-99.
8. Kagitani F, Kuroiwa Y, Wakana S, Shiroishi T, Miyoshi N, Kobayashi S, et al. Peg5/Neuronatin is an imprinted gene located on sub-distal chromosome 2 in the mouse. *Nucleic Acids Res*. 1997;25(17):3428-32.

9. Kikyo N, Williamson CM, John RM, Barton SC, Beechey CV, Ball ST, et al. Genetic and functional analysis of neuronatin in mice with maternal or paternal duplication of distal Chr 2. *Dev Biol*. 1997;190(1):66-77.

10. Sowpati DT, Thiagarajan D, Sharma S, Sultana H, John R, Surani A, et al. An intronic DNA sequence within the mouse Neuronatin gene exhibits biochemical characteristics of an ICR and acts as a transcriptional activator in Drosophila. *Mech Dev*. 2008;125(11-12):963-73.

11. Scott WR, Gelegen C, Chandarana K, Karra E, Yousseif A, Amouyal C, et al. Differential pre-mRNA splicing regulates Nnat isoforms in the hypothalamus after gastric bypass surgery in mice. *PLoS One*. 2013;8(3):e59407.

12. Tung YC, Ma M, Piper S, Coll A, O'Rahilly S, and Yeo GS. Novel leptin-regulated genes revealed by transcriptional profiling of the hypothalamic paraventricular nucleus. *J Neurosci*. 2008;28(47):12419-26.

13. Vrang N, Meyre D, Froguel P, Jelsing J, Tang-Christensen M, Vatin V, et al. The imprinted gene neuronatin is regulated by metabolic status and associated with obesity. *Obesity (Silver Spring)*. 2010;18(7):1289-96.

14. Joe MK, Lee HJ, Suh YH, Han KL, Lim JH, Song J, et al. Crucial roles of neuronatin in insulin secretion and high glucose-induced apoptosis in pancreatic beta-cells. *Cell Signal*. 2008;20(5):907-15.

15. Li X, Thomason PA, Withers DJ, and Scott J. Bio-informatics analysis of a gene co-expression module in adipose tissue containing the diet-responsive gene Nnat. *BMC Syst Biol*. 2010;4:175.

16. Suh YH, Kim Y, Bang JH, Choi KS, Lee JW, Kim WH, et al. Analysis of gene expression profiles in insulin-sensitive tissues from pre-diabetic and diabetic Zucker diabetic fatty rats. *J Mol Endocrinol*. 2005;34(2):299-315.

17. Dalgaard K, Landgraf K, Heyne S, Lempradl A, Longinotto J, Gossens K, et al. Trim28 Haploinsufficiency Triggers Bi-stable Epigenetic Obesity. *Cell*. 2016;164(3):353-64.

18. Chu K, and Tsai MJ. Neuronatin, a downstream target of BETA2/NeuroD1 in the pancreas, is involved in glucose-mediated insulin secretion. *Diabetes*. 2005;54(4):1064-73.

19. Kanno N, Higuchi M, Yoshida S, Yako H, Chen M, Ueharu H, et al. Expression studies of neuronatin in prenatal and postnatal rat pituitary. *Cell Tissue Res*. 2016;364(2):273-88.

20. Lin HH, Bell E, Uwanogho D, Perfect LW, Noristani H, Bates TJ, et al. Neuronatin promotes neural lineage in ESCs via Ca(2+) signaling. *Stem Cells*. 2010;28(11):1950-60.

21. Pitale PM, Howse W, and Gorbatyuk M. Neuronatin Protein in Health and Disease. *J Cell Physiol*. 2017;232(3):477-81.

22. Kone M, Pullen TJ, Sun G, Ibberson M, Martinez-Sanchez A, Sayers S, et al. LKB1 and AMPK differentially regulate pancreatic beta-cell identity. *FASEB J*. 2014;28(11):4972-85.

23. Thorens B, Tarussio D, Maestro MA, Rovira M, Heikkila E, and Ferrer J. Ins1(Cre) knock-in mice for beta cell-specific gene recombination. *Diabetologia*. 2015;58(3):558-65.

24. Miyazaki J, Araki K, Yamato E, Ikegami H, Asano T, Shibasaki Y, et al. Establishment of a pancreatic beta cell line that retains glucose-inducible insulin secretion: special reference to expression of glucose transporter isoforms. *Endocrinology*. 1990;127(1):126-32.

25. Liu M, Hodish I, Haataja L, Lara-Lemus R, Rajpal G, Wright J, et al. Proinsulin misfolding and diabetes: mutant INS gene-induced diabetes of youth. *Trends Endocrinol Metab*. 2010;21(11):652-9.

26. Liu M, Sun J, Cui J, Chen W, Guo H, Barbetti F, et al. INS-gene mutations: from genetics and beta cell biology to clinical disease. *Mol Aspects Med*. 2015;42:3-18.

27. Iezzi M, Regazzi R, and Wollheim CB. The Rab3-interacting molecule RIM is expressed in pancreatic beta-cells and is implicated in insulin exocytosis. *FEBS Lett*. 2000;474(1):66-70.

28. Evans EA, Gilmore R, and Blobel G. Purification of microsomal signal peptidase as a complex. *Proc Natl Acad Sci U S A*. 1986;83(3):581-5.

29. Jackson RC, and Blobel G. Post-translational cleavage of presecretory proteins with an extract of rough microsomes from dog pancreas containing signal peptidase activity. *Proc Natl Acad Sci U S A*. 1977;74(12):5598-602.

30. Kalies KU, and Hartmann E. Membrane topology of the 12- and the 25-kDa subunits of the mammalian signal peptidase complex. *J Biol Chem*. 1996;271(7):3925-9.

31. Shelness GS, Lin L, and Nicchitta CV. Membrane topology and biogenesis of eukaryotic signal peptidase. *J Biol Chem*. 1993;268(7):5201-8.

32. Dancourt J, and Barlowe C. Protein sorting receptors in the early secretory pathway. *Annu Rev Biochem*. 2010;79:777-802.

33. Zanetti G, Pahuja KB, Studer S, Shim S, and Schekman R. COPII and the regulation of protein sorting in mammals. *Nat Cell Biol*. 2011;14(1):20-8.

34. Auclair SM, Bhanu MK, and Kendall DA. Signal peptidase I: cleaving the way to mature proteins. *Protein Sci*. 2012;21(1):13-25.

35. Liu M, Wright J, Guo H, Xiong Y, and Arvan P. Proinsulin entry and transit through the endoplasmic reticulum in pancreatic beta cells. *Vitam Horm*. 2014;95:35-62.

36. Bohni PC, Deshaies RJ, and Schekman RW. SEC11 is required for signal peptide processing and yeast cell growth. *J Cell Biol*. 1988;106(4):1035-42.

37. Shelness GS, and Blobel G. Two subunits of the canine signal peptidase complex are homologous to yeast SEC11 protein. *J Biol Chem*. 1990;265(16):9512-9.

38. Antonin W, Meyer HA, and Hartmann E. Interactions between Spc2p and other components of the endoplasmic reticulum translocation sites of the yeast Saccharomyces cerevisiae. *J Biol Chem*. 2000;275(44):34068-72.

39. Fang H, Panzner S, Mullins C, Hartmann E, and Green N. The homologue of mammalian SPC12 is important for efficient signal peptidase activity in Saccharomyces cerevisiae. *J Biol Chem*. 1996;271(28):16460-5.

40. Mullins C, Meyer HA, Hartmann E, Green N, and Fang H. Structurally related Spc1p and Spc2p of yeast signal peptidase complex are functionally distinct. *J Biol Chem*. 1996;271(46):29094-9.

41. Zhang R, Miner JJ, Gorman MJ, Rausch K, Ramage H, White JP, et al. A CRISPR screen defines a signal peptide processing pathway required by flaviviruses. *Nature*. 2016;535(7610):164-8.

42. Guo H, Xiong Y, Witkowski P, Cui J, Wang LJ, Sun J, et al. Inefficient translocation of preproinsulin contributes to pancreatic beta cell failure and late-onset diabetes. *J Biol Chem*. 2014;289(23):16290-302.

43. Liu M, Lara-Lemus R, Shan SO, Wright J, Haataja L, Barbetti F, et al. Impaired cleavage of preproinsulin signal peptide linked to autosomal-dominant diabetes. *Diabetes*. 2012;61(4):828-37.

44. Edghill EL, Flanagan SE, Patch AM, Boustred C, Parrish A, Shields B, et al. Insulin mutation screening in 1,044 patients with diabetes: mutations in the INS gene are a common cause of neonatal diabetes but a rare cause of diabetes diagnosed in childhood or adulthood. *Diabetes*. 2008;57(4):1034-42.

45. Meur G, Simon A, Harun N, Virally M, Dechaume A, Bonnefond A, et al. Insulin gene mutations resulting in early-onset diabetes: marked differences in clinical presentation, metabolic status, and pathogenic effect through endoplasmic reticulum retention. *Diabetes*. 2010;59(3):653-61.

46. Stoy J, Edghill EL, Flanagan SE, Ye H, Paz VP, Pluzhnikov A, et al. Insulin gene mutations as a cause of permanent neonatal diabetes. *Proc Natl Acad Sci U S A*. 2007;104(38):15040-4.

47. Rutter GA, Pullen TJ, Hodson DJ, and Martinez-Sanchez A. Pancreatic beta-cell identity, glucose sensing and the control of insulin secretion. *Biochem J*. 2015;466(2):203-18.

48. Choudhury AI, Heffron H, Smith MA, Al-Qassab H, Xu AW, Selman C, et al. The role of insulin receptor substrate 2 in hypothalamic and beta cell function. *J Clin Invest*. 2005;115(4):940-50.

49. Cantley J, Choudhury AI, Asare-Anane H, Selman C, Lingard S, Heffron H, et al. Pancreatic deletion of insulin receptor substrate 2 reduces beta and alpha cell mass and impairs glucose homeostasis in mice. *Diabetologia*. 2007;50(6):1248-56.

50. Ravier MA, and Rutter GA. Isolation and culture of mouse pancreatic islets for ex vivo imaging studies with trappable or recombinant fluorescent probes. *Methods Mol Biol*. 2010;633:171-84.

51. Carrat GR, Hu M, Nguyen-Tu MS, Chabosseau P, Gaulton KJ, van de Bunt M, et al. Decreased STARD10 Expression Is Associated with Defective Insulin Secretion in Humans and Mice. *Am J Hum Genet*. 2017;100(2):238-56.

52. Asfari M, Janjic D, Meda P, Li G, Halban PA, and Wollheim CB. Establishment of 2-mercaptoethanol-dependent differentiated insulin-secreting cell lines. *Endocrinology*. 1992;130(1):167-78.

Figures and figure legends

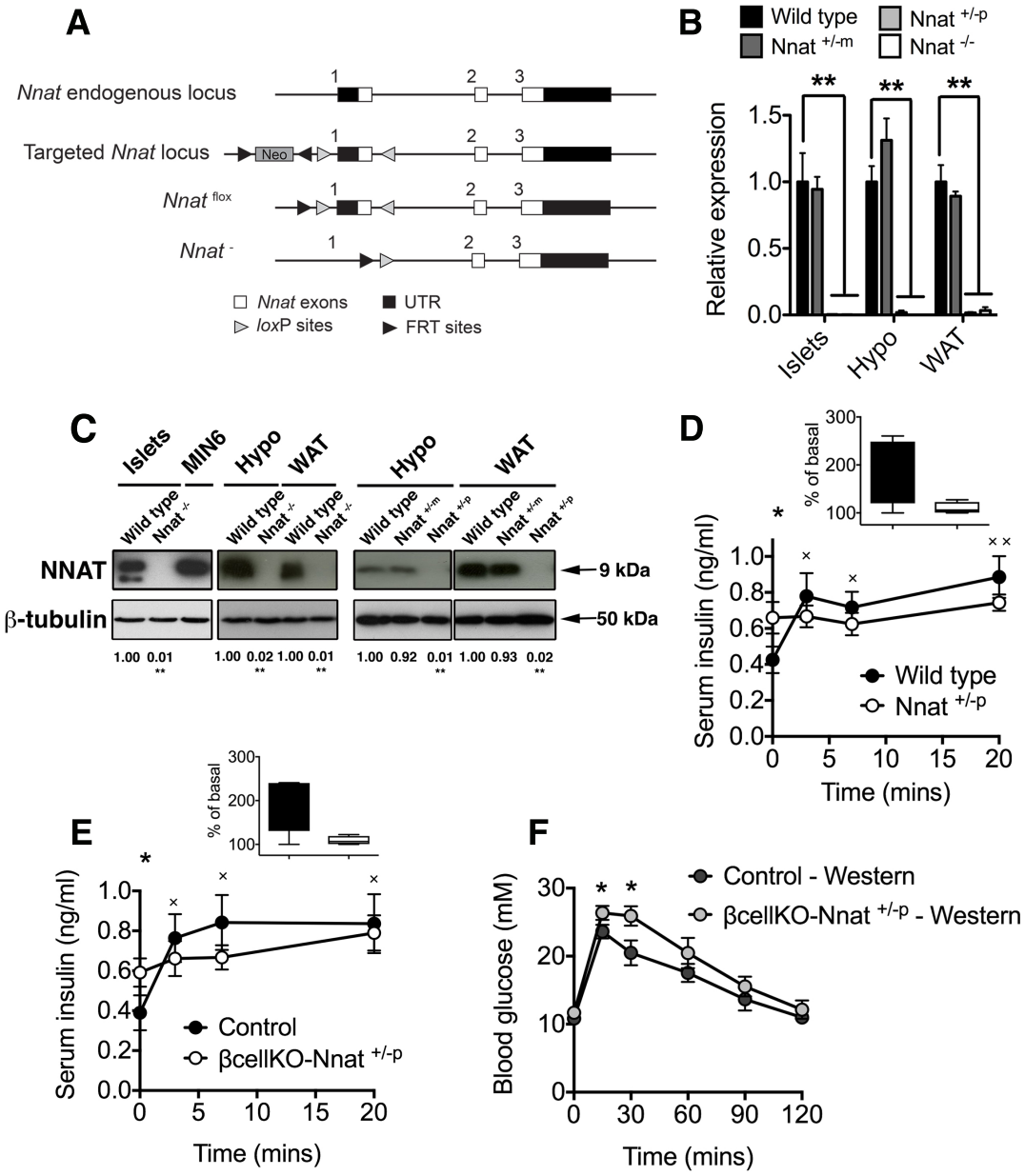

Figure 1. Effect of *Nnat* deficiency *in vivo*. (**A**) Targeted inactivation of the *Nnat* gene. Exon 1 was flanked by *lox*P sites with the *neomycin* selection cassette (Neo) flanked by FRT sites, to produce a floxed and null allele. (**B**, **C**) Quantitative RT-PCR and representative Western blot analysis of *Nnat* expression in tissues of wild type, heterozygous $Nnat^{+/-m}$ (maternal deletion), heterozygous $Nnat^{+/-p}$ (paternal deletion) and homozygous $Nnat^{-/-}$ mice on C57BL/6J background. *Hprt* (for Islets and Hypothalamus (Hypo)) and *Cyclophilin A* (for WAT) mRNA were used as internal

controls. β-tubulin served as a loading control for protein expression and data is expressed as mean of fold change compared to wild type mice (n = 4-7 animals per group and n = 4 for RT-PCR and Western blot respectively). (**D, E)** Measurement of insulin secretion *in vivo* in response to i.p. glucose in *Nnat*$^{+/-p}$ vs wild type (**D**) and βcellKO-*Nnat*$^{+/-p}$ vs control (**E**) mice on C57BL/6J background (n = 9 and n = 8 animals per genotype respectively). Inset shows box and whiskers plot of the same data plotted as percentage insulin secretion across all time points compared with basal insulin values (at T = 0). (x = $p < 0.05$ and xx = $p < 0.01$ indicate statistically significant increases in secretion in wild type mice compared with basal insulin values). (**F**) Glucose tolerance in Western diet-fed wild type and βcellKO-*Nnat*$^{+/-p}$ mice (C57BL/6J) (n = 10 mice per genotype). In all panels, data is represented as mean ± SEM (* $p < 0.05$, ** $p < 0.01$).

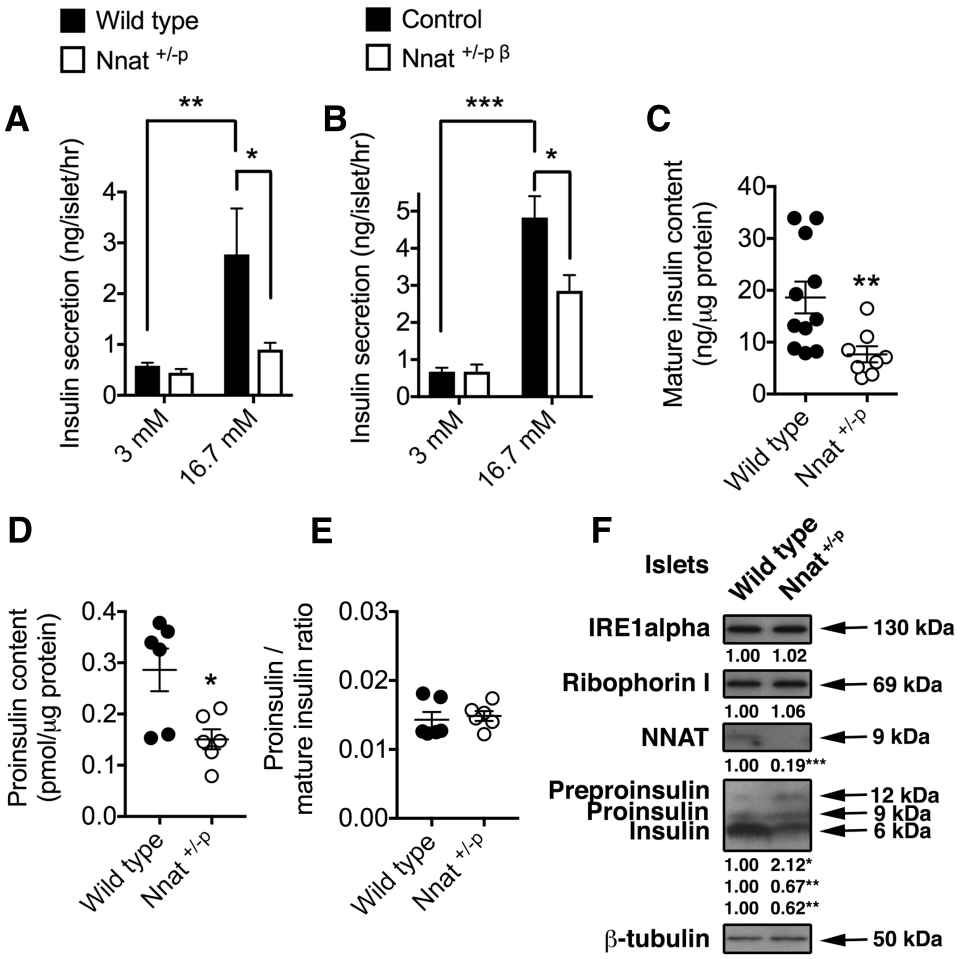

Figure 2. Insulin content and secretion in *Nnat* deficient islets. (**A**) Insulin secretion in static incubations of primary isolated islets from *Nnat*$^{+/-p}$ and wild type mice was determined *in vitro* under low (3 mM) and high (16.7 mM) glucose conditions (n = 12 animals per group). (**B**) Insulin secretion in static incubations of primary isolated islets from control and βcellKO-*Nnat*$^{+/-p}$ mice was determined as in **A** (n = 8 mice per genotype). (**C-E**) Mature insulin content (n = 11 for wild type and 8 for *Nnat*$^{+/-p}$), (**C**) proinsulin content (**D**) and proinsulin to mature insulin ratio (**E**) (both n = 6 animals per group) were quantified and calculated in isolated islets from wild type and *Nnat*$^{+/-p}$ mice and normalised to total protein. (**F**) Western blotting analysis of protein levels in primary isolated islets from *Nnat*$^{+/-p}$ and wild type mice. A representative blot of 2 independent experiments (n = 4 mice per genotype) is shown. β-tubulin was used as a loading control and data is expressed as mean of fold change compared to wild type mice. In all panels, data is expressed as mean ± SEM (* $p < 0.05$, ** $p < 0.01$, *** $p < 0.001$).

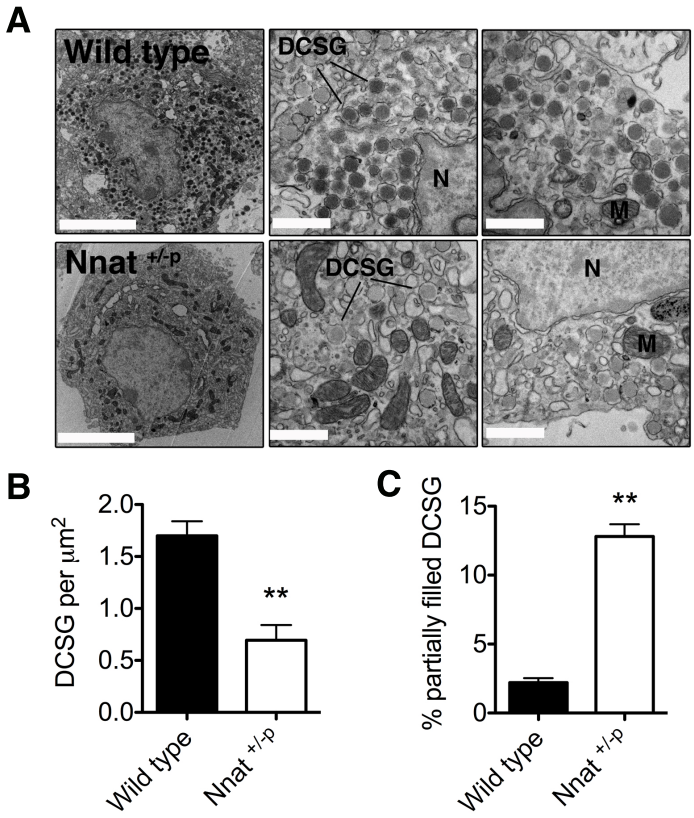

Figure 3. Insulin secretory granule morphology in *Nnat* deficient beta cells by EM. (**A**) (Left) Representative electron micrographs (EM) of beta cells from wild type and *Nnat*$^{+/-p}$ mice in ultra-thin sections (scale bar = 5 μm). (Middle, Right) Higher magnification images showing dense core secretory granules (DCSG), nuclei (N) and various mitochondria (M) (scale bar = 1 μm). A total of 9 beta cells from sections of fixed islets was analysed from 3 different animals per genotype. (**B, C**) Quantification of the number of DCSG per unit area, and also percentage of partially filled DCSG, using EM images from wild type and *Nnat*$^{+/-p}$ beta cells in **A**. In all panels, data is expressed as mean ± SEM (** $p < 0.01$).

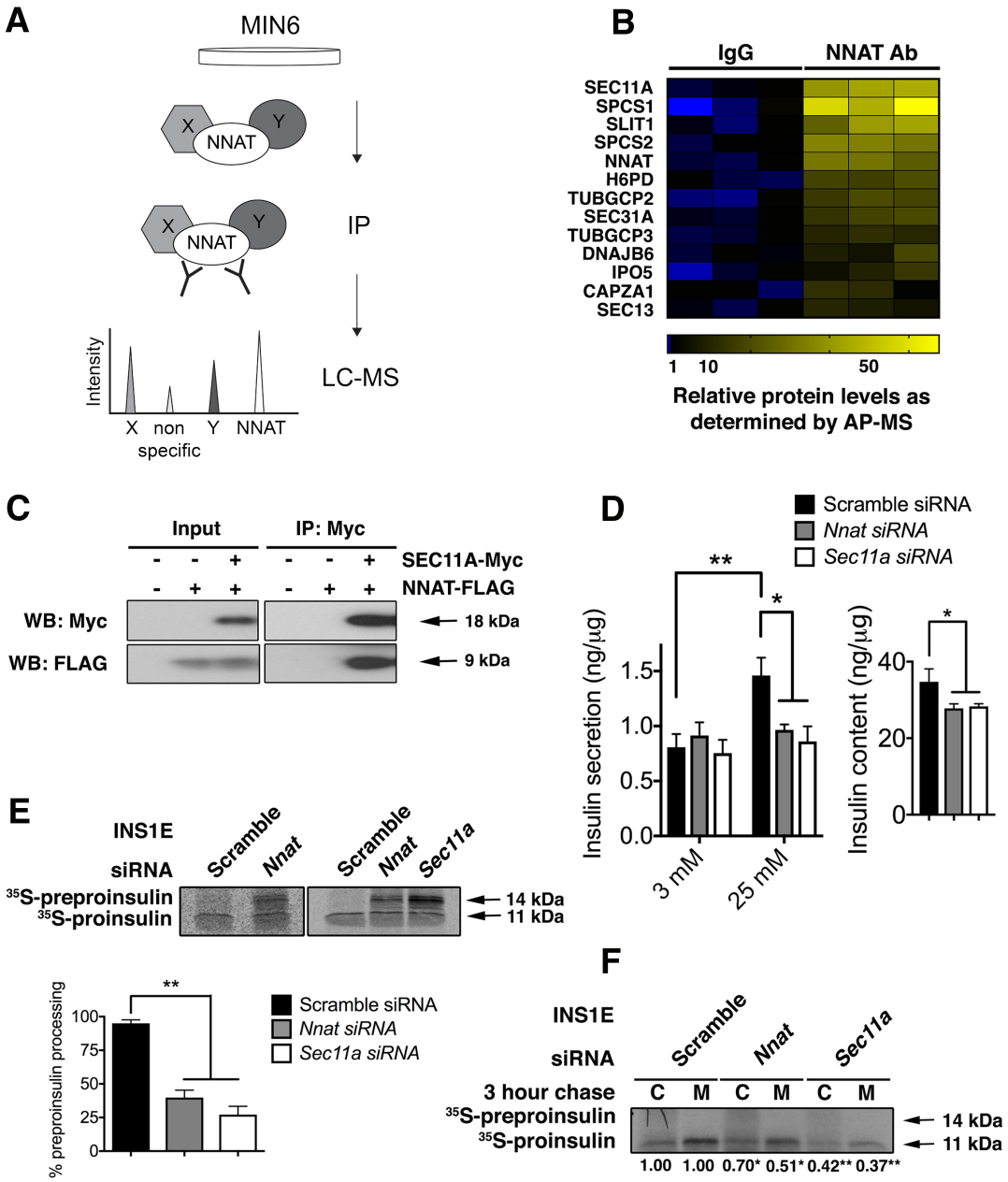

Figure 4. NNAT interacts with the SPC to modulate preproinsulin handling (**A**) Overview of Affinity Purification-Mass Spectrometry (AP-MS) screen for novel interaction partners of NNAT. Endogenous NNAT was immunoprecipitated (IP) from MIN6 cell lysates and interacting partners in co-IPs analysed by Liquid Chromatography-Mass Spectrometry (LC-MS) (**B**) Heatmap obtained from AP-MS analysis of top protein hits found in IPs using antibodies against NNAT (NNAT Ab) and control IPs with rabbit immunoglobulins (IgG). Relatively high abundance is shown in yellow and relatively low abundance in blue. (**C**) Lysates from HEK293T

cells transfected with plasmids encoding c-Myc tagged SEC11A and FLAG-tagged NNAT were immunoprecipitated using anti c-Myc antibodies. Proteins in input and IP samples were detected by Western blotting using anti c-Myc and anti-FLAG antibodies. Panel shows a representative blot of 3 independent experiments. (**D**) INS1E cells transiently transfected with siRNA targeting *Nnat* and *Sec11a* were assayed *in vitro* for GSIS at low (3 mM) and high (25 mM) glucose. A scramble siRNA served as a control with data expressed as mean insulin secretion per unit cellular protein ± SEM. Inset shows total insulin content in cell lysates (n = 9 independent cultures per group). (**E**) INS1E cells transfected with c-Myc tagged preproinsulin and siRNAs targeting *Nnat* and *Sec11a* were pulse-labelled with ^{35}S-Cys/Met. Lysates were immunoprecipitated with anti-c-Myc agarose and analysed by autoradiography. Associated bar chart shows preproinsulin and proinsulin band intensities in multiple experiments quantified by densitometry and expressed as percentage processing of preproinsulin (n = 3 cultures per group from 3 independent experiments). (**F**) Similar experiments performed as in **E**, from cell lysates (C) and 3-hour chase media (M). Quantitative values for each siRNA are shown below the panel, quantified as in **E** (n = 4 cultures per group from 3 independent experiments). (* $p < 0.05$, ** $p < 0.01$).

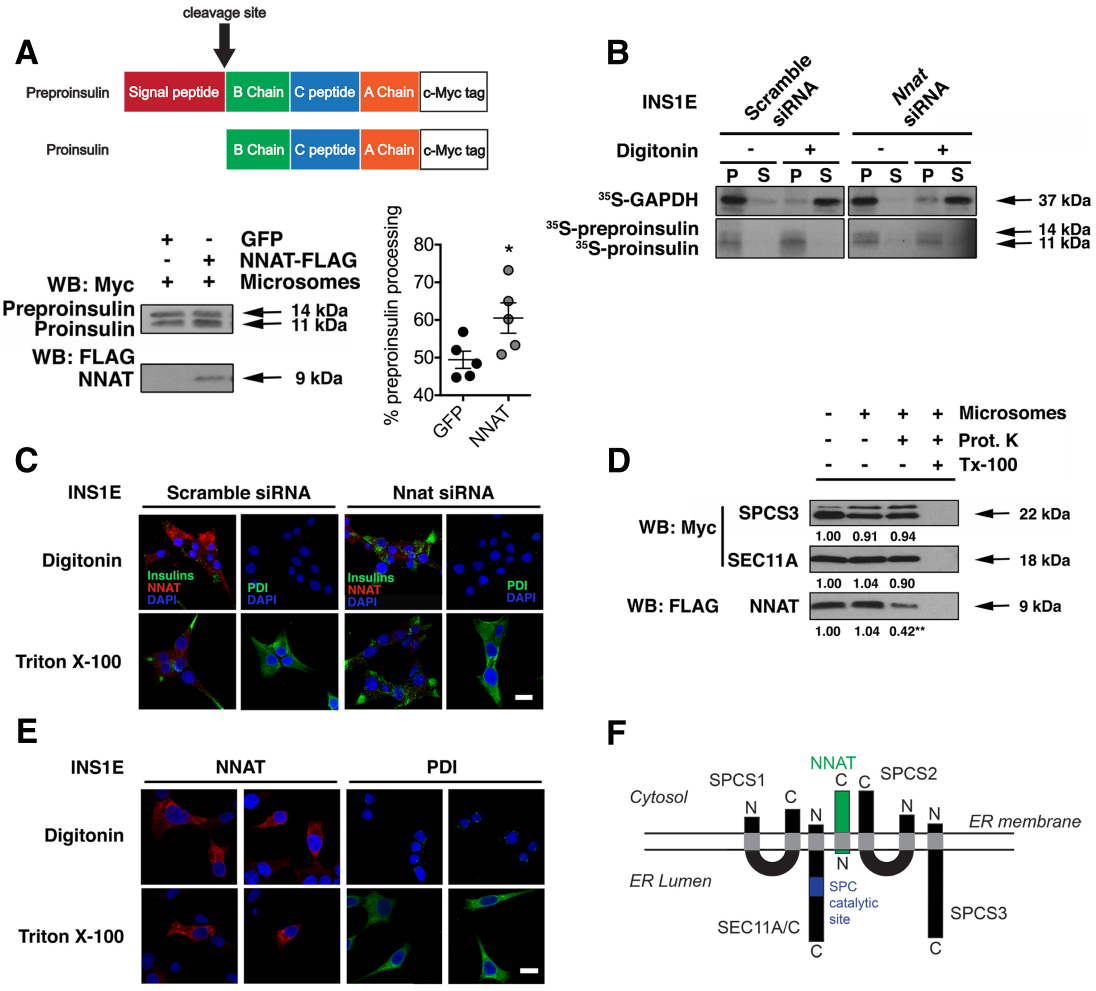

Figure 5. ER membrane topology of NNAT and its direct effect on SPC processing (**A**) Representative Western blotting analysis of *in vitro* translated preproinsulin converted to proinsulin in the presence (+) of pancreatic microsomes with and without co-expression of NNAT, expressed as percentage processing of preproinsulin ± SEM. Co-expression of GFP was used as a control. (n = 5 reactions per group, * $p < 0.05$). (**B**) Targeting of c-Myc-tagged preproinsulin to the ER membrane assessed in INS1E with *Nnat* siRNA knockdown. Cells were pulse-labelled with ^{35}S-Cys/Met, treated with digitonin and the supernatant (S) and pellet (P) fractions immunoprecipitated with anti-c-Myc and analysed by autoradiography, with a representative image shown (n = 3 independent cultures per group/treatment). (**C**) INS1E cells with *Nnat* siRNA knockdown were permeabilised with digitonin or

Triton X-100, immunostained using antibodies against preproinsulin/mature insulin (Insulins, green) and NNAT (red) and visualized by confocal microscopy. The luminal ER protein PDI (green) was used to assess membrane permeabilisation and nuclei were visualized with DAPI. Scale bar = 10 μm. (**D**) Representative Western blotting analysis of C-terminal c-Myc tagged SPCS3 and SEC11A, and FLAG tagged NNAT translated *in vitro* in the presence (+) or absence (-) of pancreatic microsomes and treated with proteinase K (Prot. K) (n = 3 reactions per group, mean ± SEM vs (-) microsomes, ** $p < 0.01$). (**E**) Immunofluorescent staining of INS1E cells permeabilised with digitonin or Triton X-100 and using antibodies against NNAT (red) and PDI (green) visualized by confocal microscopy. PDI was used to assess membrane permeabilisation and nuclei were visualized with DAPI. Scale bar = 10 μm. (**F**) Topology of NNAT (green) and subunits of the SPC (black) on the ER membrane. The catalytic site for signal peptidase cleavage in SEC11A/C is shown in blue (N and C: amino and carboxy-terminal respectively).

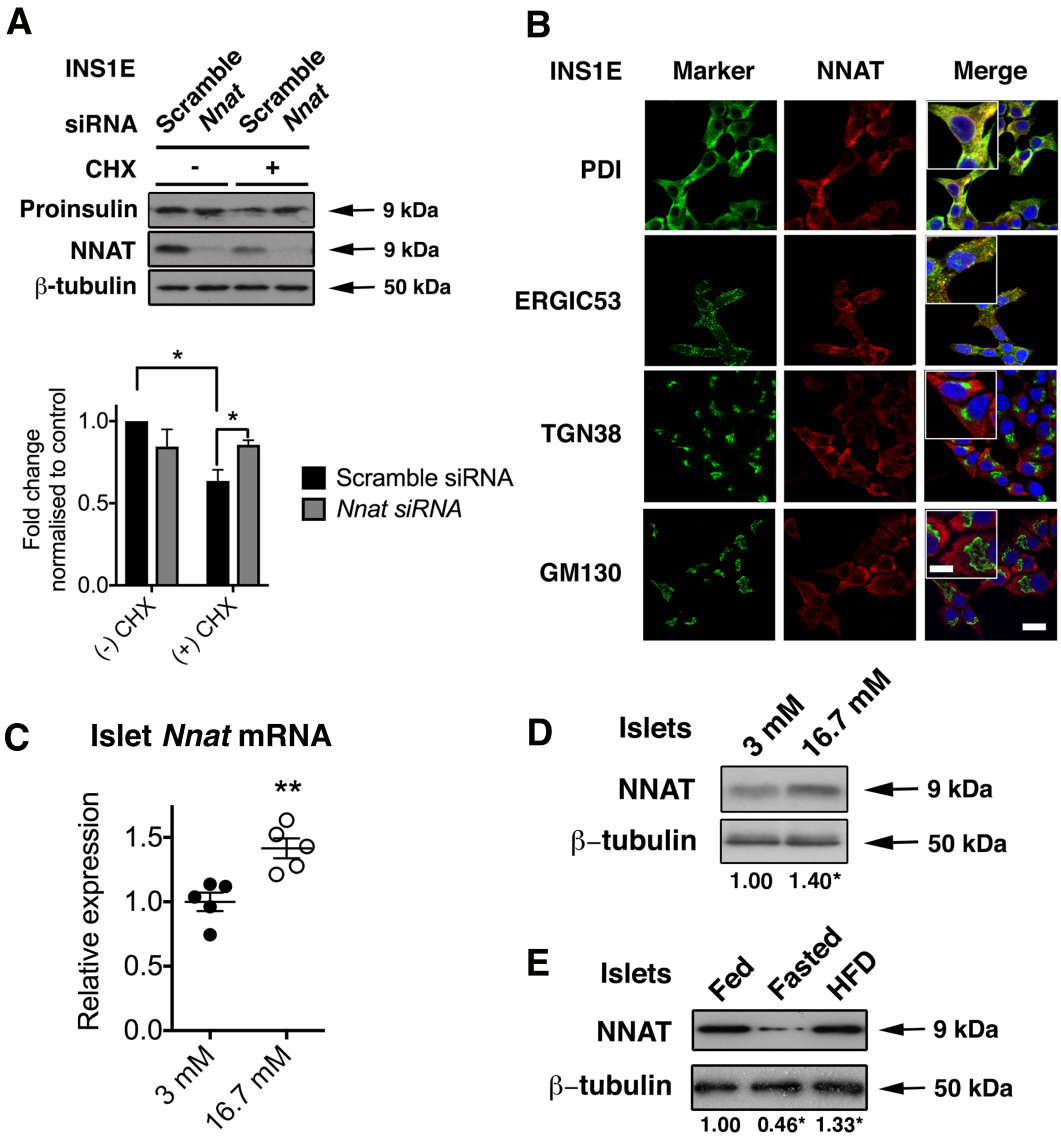

Figure 6. Effect of NNAT on efficiency of proinsulin ER exit and regulation of NNAT expression by glucose (**A**) Western blotting analysis of proinsulin protein levels in INS1E transiently transfected with siRNA targeting *Nnat* and treated with cycloheximide (CHX). A scramble siRNA and β-tubulin served as controls. Associated bar chart shows proinsulin band intensities in multiple experiments quantified by densitometry and expressed as fold change ± SEM of expression relative to untreated scramble siRNA samples. A representative blot of 3 independent experiments is shown (n = 4 independent cultures per group, * $p < 0.05$). (**B**) Immunofluorescent staining of INS1E cells using antibodies against NNAT (red) and

various subcellular localization markers (green) visualized by confocal microscopy. Nuclei were visualized with DAPI. Scale bar = 10 μm. Inset shows part of merged images with 2x digital zoom, scale bar = 5 μm. (**C**) Quantitative RT-PCR analysis of *Nnat* mRNA in isolated islets from wild type C57BL/6J mice cultured in low (3 mM) or high (16.7 mM) glucose conditions for 6 hours. *Hprt* mRNA was used as an internal control and data is represented as mean of fold change ± SEM compared to 3 mM cultures (n = 5 animals per group). (**D**) Parallel islet preps receiving the same treatment as in **C** were analysed for protein expression by Western blotting. β-tubulin was used as a loading control. (**E**) Representative Western (immuno-) blot analysis of NNAT protein expression in isolated pancreatic islets of wild type C57BL/6J mice fasted overnight (Fasted) or fed HFD for 72 hours (HFD). Values for each condition are shown below each panel, as mean fold change ± SEM compared with chow fed mice (Fed). β-tubulin was used as a loading control (n = 5 animals per group) (* $p < 0.05$, ** $p < 0.01$).

Supplemental data

Figures and figure legends

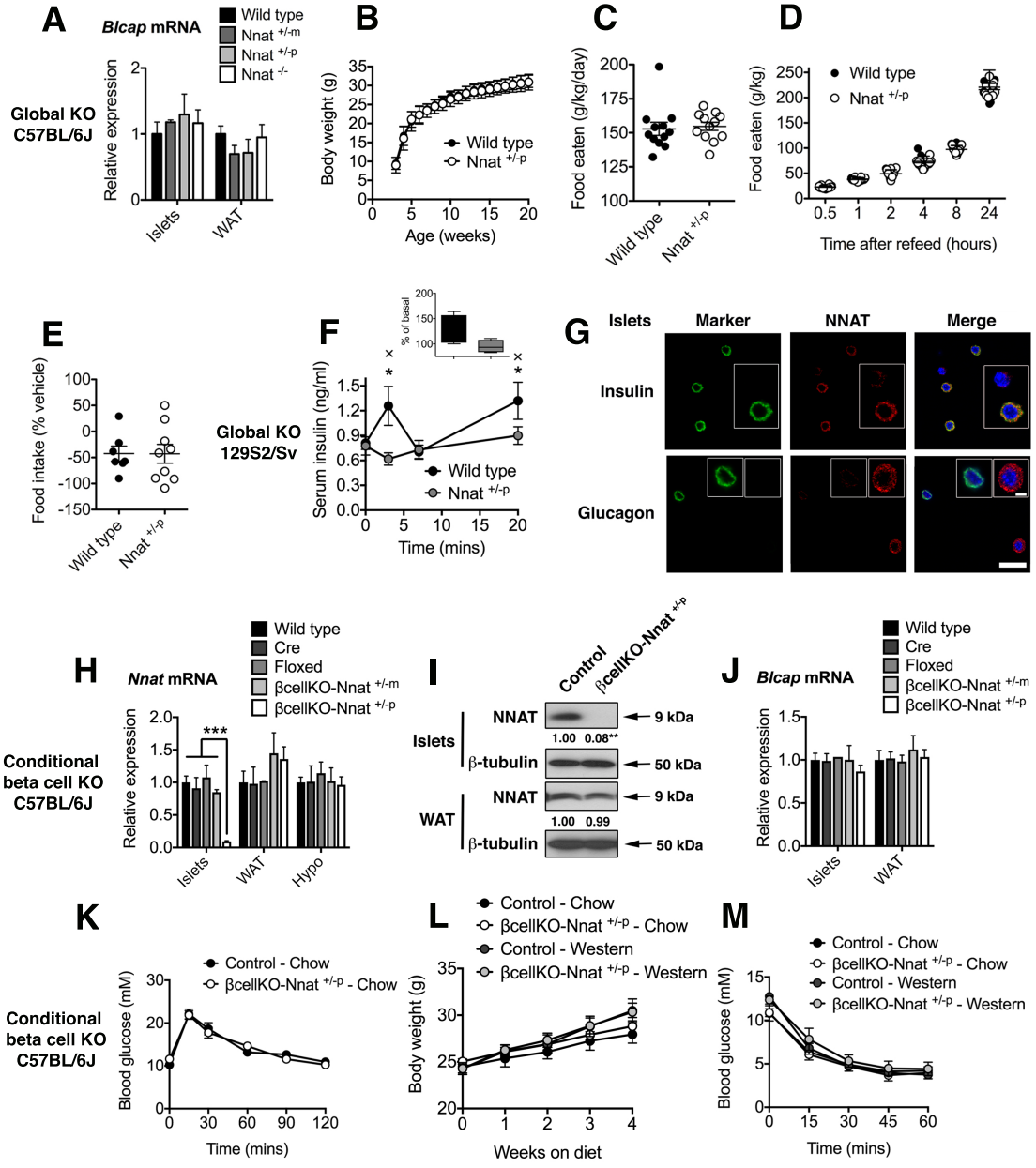

Supplemental Figure 1. Metabolic profiling of *Nnat* deficient mice. (**A**) RT-PCR analysis of *Blcap* mRNA expression in isolated islets and WAT of wild type, heterozygous $Nnat^{+/-m}$ (maternal deletion), heterozygous $Nnat^{+/-p}$ (paternal deletion) and homozygous $Nnat^{-/-}$ mice on C57BL/6J background. *Hprt* and *Cyclophilin A* mRNA was used as an internal control for islets and WAT respectively and data is

represented as mean of fold change ± SEM compared to wild type mice (n = 6 animals per genotype). (**B**) Body weights of wild type and *Nnat*$^{+/-p}$ mice on C57BL/6J background (n = 19 and 23 for wild type and *Nnat*$^{+/-p}$ mice respectively. (**C, D**) *Ad libitum* feeding (**C**) and feeding following an overnight fast (**D**) in wild type and *Nnat*$^{+/-p}$ mice (C57BL/6J) (n = 12 animals per genotype). (**E**) Food intake alterations (percentage change) in response to exogenous leptin compared to internal saline crossover control in wild type and *Nnat*$^{+/-p}$ mice (C57BL/6J) (n = 7 and 9 for wild type and *Nnat*$^{+/-p}$ mice respectively). (**F**) Measurement of insulin secretion *in vivo* in response to i.p. glucose in *Nnat*$^{+/-p}$ mice on 129S2/Sv background (n = 10 animals per genotype). Inset shows box and whiskers plot of the same data plotted as percentage insulin secretion across all time points compared with basal insulin values (at T = 0), demonstrating the dispersion of insulin secretion increase in wild type animals across all time points that was completely lacking in *Nnat*$^{+/-p}$ mice (x = $p < 0.05$, indicating statistically significant increases in secretion in wild type mice at each time point compared with basal insulin values). (**G**) Immunofluorescent staining of dispersed islet cells using antibodies against NNAT (red) and markers of beta (Insulin, green) and alpha (Glucagon, green) cells assessed by confocal microscopy. Nuclei were visualized with DAPI. Scale bar = 25 μm. Inset shows individual cells with 2x digital zoom, scale bar = 5 μm. (**H, I**) RT-PCR and representative Western blot analysis of *Nnat* expression in isolated islets, WAT and Hypothalamus (Hypo) in wild type, *Ins1Cre* positive (Cre), *Nnat*$^{+/flox}$ (Floxed), *Ins1Cre* positive *Nnat*$^{+/flox}$ from maternal allele (βcellKO-*Nnat*$^{+/-m}$) and *Ins1Cre* positive *Nnat*$^{+/flox}$ from paternal allele (βcellKO-*Nnat*$^{+/-p}$) mice on C57BL/6J background. *Hprt* (Islets and Hypo) and *Cyclophilin A* (WAT) mRNA were used as internal controls, and data is represented as mean of fold change ± SEM compared to wild type mice. β-tubulin was used as a protein loading

control (n = 8 and n = 4 animals per genotype for RT-PCR and Western blot respectively). (**J**) RT-PCR analysis of *Blcap* mRNA expression in isolated islets and WAT in the same mice as **H**. (**K, L, M**) Glucose tolerance, body weights and insulin sensitivity in chow and Western diet fed wild type and βcellKO-*Nnat*$^{+/-p}$ mice (C57BL/6J) (n = 5 and 10 mice for chow and Western diet per genotype respectively). In all panels, results are shown as mean ± SEM (* $p < 0.05$, ** $p < 0.01$, *** $p < 0.001$).

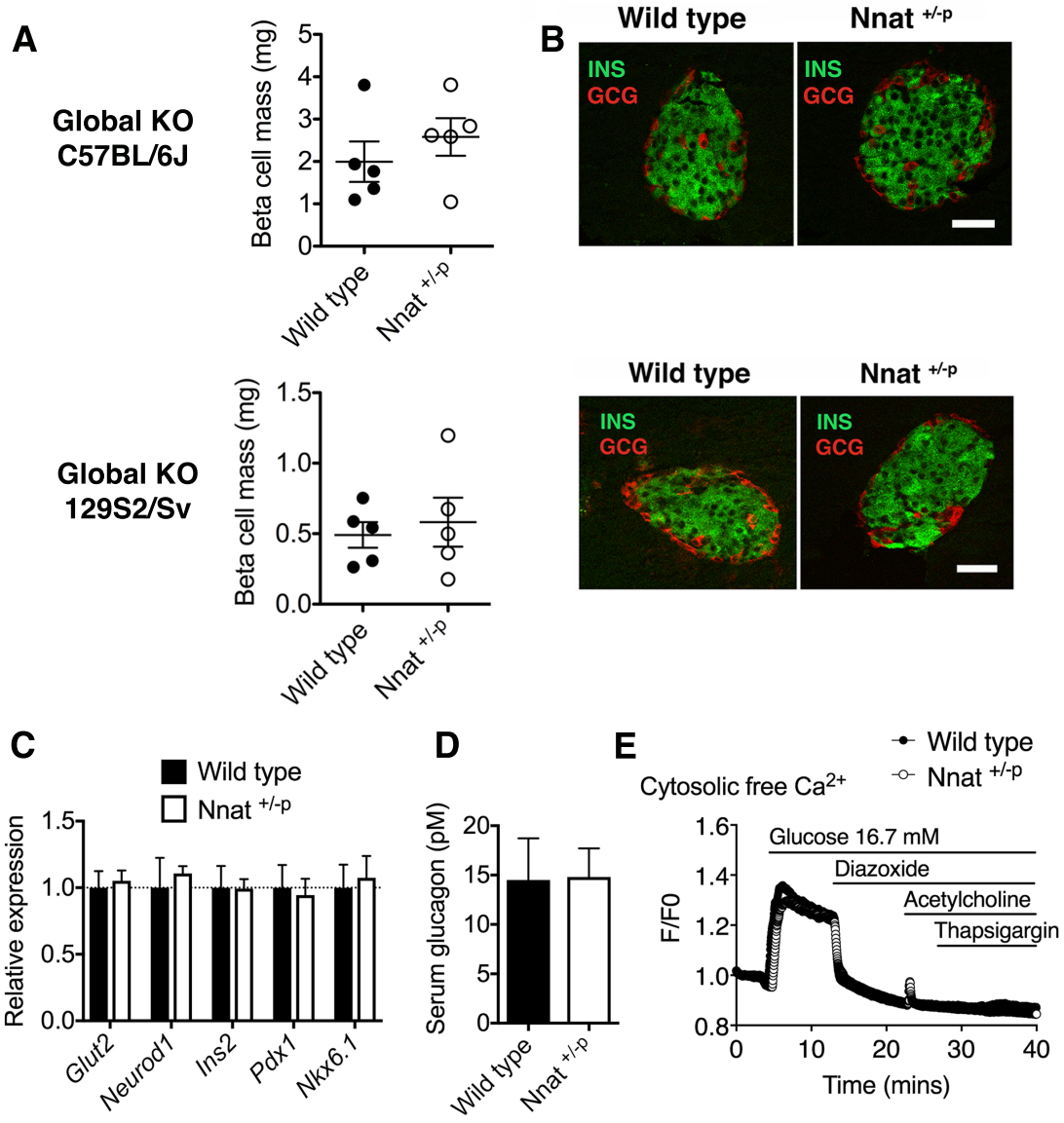

Supplemental Figure 2. Assessment of islet function upon *Nnat* deletion. (**A, B**) Morphometric analysis of β-cell mass (**A**) in pancreatic sections from wild type and *Nnat*$^{+/-p}$ mice on C57BL/6J and 129S2/Sv background (n = 5 animals per genotype) with representative immunofluorescent images (**B**) showing staining of insulin (INS, green) and glucagon (GCG, red). Scale bar = 25 μm. (**C**) Quantitative RT-PCR analysis of mRNAs encoding key beta cell genes in isolated islets of wild type and *Nnat*$^{+/-p}$ mice. *Hprt* mRNA expression was used as an internal control and data is represented relative to wild type mice (n = 6 animals per genotype). (**D**) Glucagon levels in serum of fasted wild type and *Nnat*$^{+/-p}$ mice (C57BL/6J) (n = 9 mice per genotype). (**E**) Ca^{2+}-bound Fluo-2 fluorescence in response to high glucose (16.7 mM) and other agents in primary islets expressed as normalised intensity over time (F / F0) (n = 18 islets total from 6 mice per genotype). In all panels, results are shown as mean ± SEM.

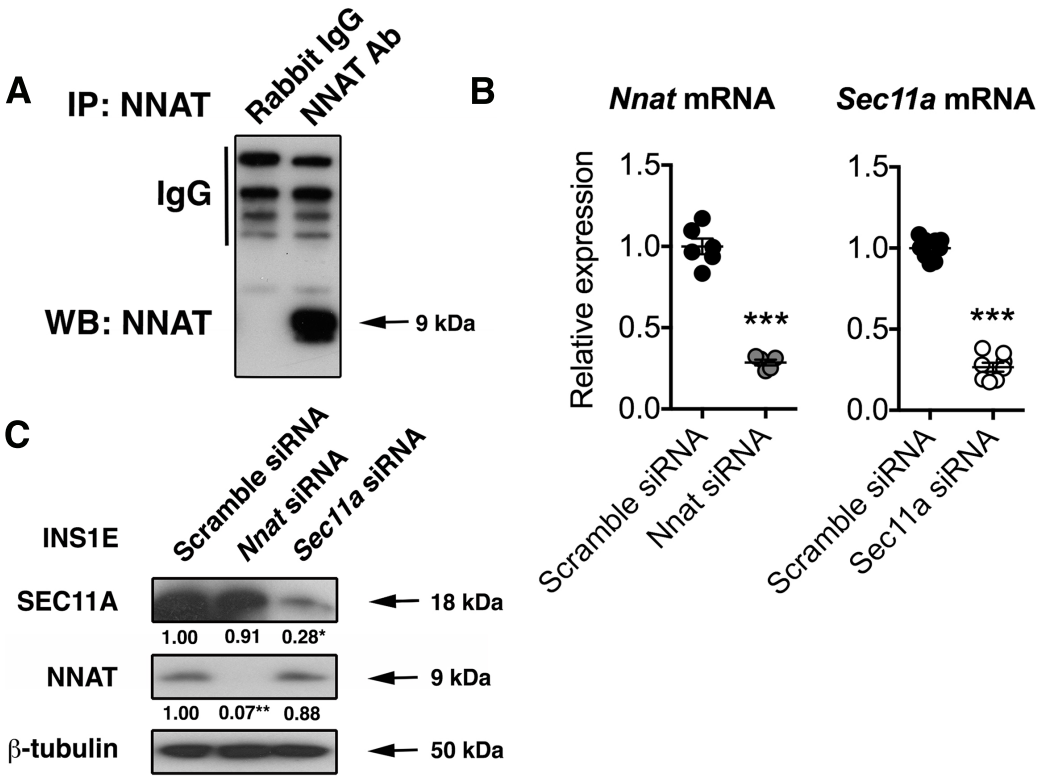

Supplemental Figure 3. NNAT immunoprecipitation and knockdown. (**A**) MIN6 cell lysates were immunoprecipitated with antibodies against NNAT (NNAT Ab) or rabbit IgG as a control, with Western blotting (representative blot shown) used to check the presence of endogenous NNAT in immunoprecipitates. (**B**) Quantitative RT-PCR analysis of mRNA encoding *Nnat* and *Sec11a* in INS1E cells transfected with control (Scramble), *Nnat* or *Sec11a* siRNA. *Hprt* expression was used as an internal control and data is expressed as fold change ± SEM vs scramble controls (n = 6 and 9 independent cultures per group for *Nnat* and *Sec11a* respectively). (**C**) INS1E cells with siRNA-mediated knockdown of *Nnat* and *Sec11a* as in **B** were analysed by Western blotting for expression of these proteins. β-tubulin was used as a loading control and a representative blot is shown (* $p < 0.05$, ** $p < 0.01$, *** $p < 0.001$).

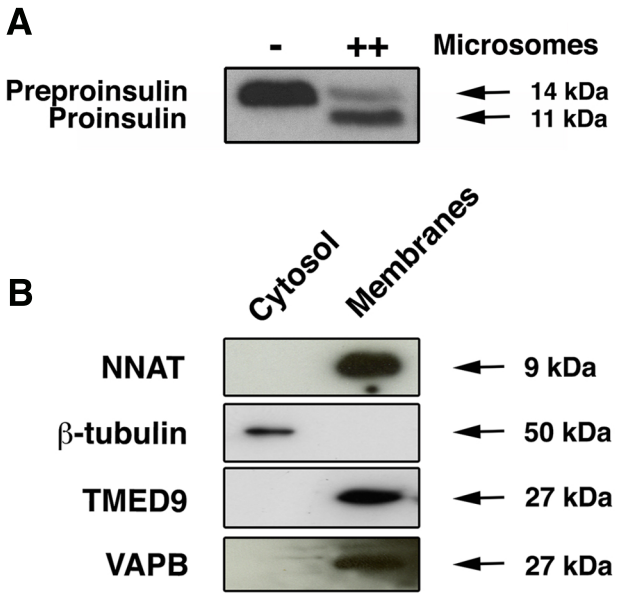

Supplemental Figure 4. ***In vitro*** **peptidase assay and NNAT as a transmembrane protein. (A)** Representative Western blotting analysis of *in vitro* translated c-Myc tagged preproinsulin converted to proinsulin in the presence (++) or absence (-) of pancreatic microsomes (containing endogenous signal peptidase activity). (**B**) A crude membrane fraction was prepared from clarified INS1E cell lysates with proteins from the high speed pellet (Membranes) and supernatant (Cytosol) fractions analysed by Western blotting using antibodies against NNAT, β-tubulin, TMED9 and VAPB.

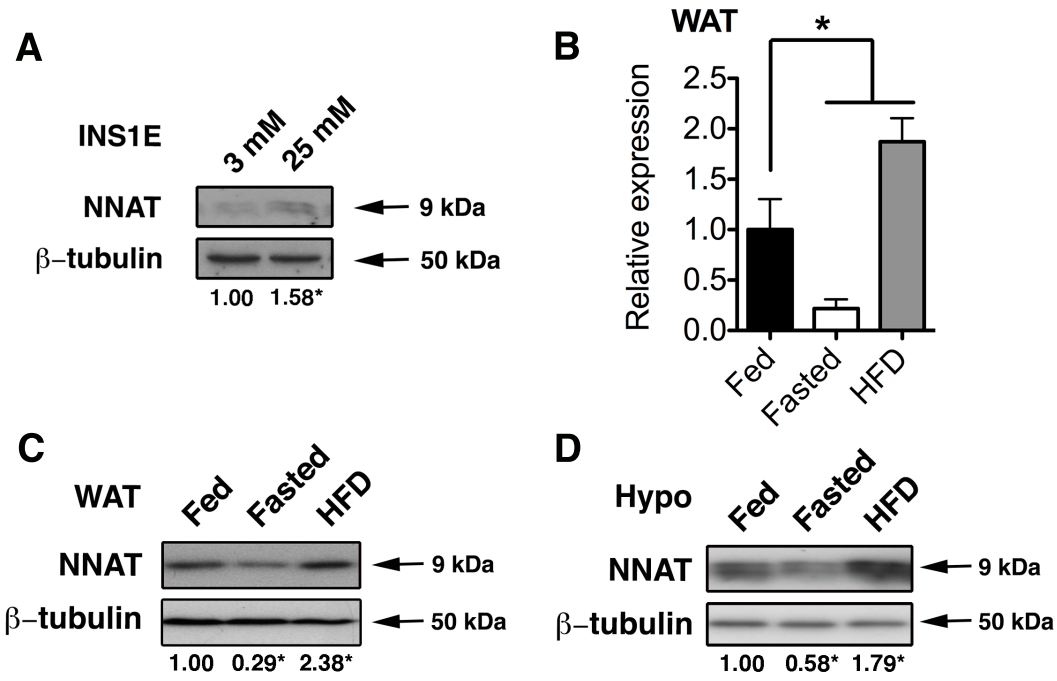

Supplemental Figure 5. NNAT regulation by glucose and the diet. (**A**) Representative Western blotting analysis of NNAT protein expression in INS1E cells cultured in low (3 mM) or high (25 mM) glucose conditions for 6 hours. Values for each condition are shown below the panel, as mean of fold change compared with low glucose controls. β-tubulin was used as a loading control (n = 6 independent cultures per treatment). (**B**) Quantitative RT-PCR analysis of *Nnat* mRNA in WAT from wild type C57BL/6J mice fasted overnight (Fasted) or acutely fed HFD for 72 hours (HFD) vs chow fed controls (Fed). *Cyclophilin A* mRNA was used as an internal control. (**C**) Western blot analysis of NNAT protein expression in the same tissues with β-tubulin used as a loading control (n = 5 animals per group). (**D**) Representative Western blot analysis of NNAT protein expression in the hypothalamus (Hypo) of the same mice used in **C**. In all panels, results are shown as mean ± SEM (* $p < 0.05$)

Supplemental Table 2.	
List of plasmids and RT-PCR probes	
Plasmids	**Source**
Expression in cell lines:	
pcDNA3.1-*Nnat*-FLAG	This paper
In vitro translation:	
pT7CFE1-*Preproinsulin II*-Myc	This paper
pT7CFE1-*Spcs3*-Myc	This paper
pT7CFE1-*Sec11a*-Myc	This paper
pT7CFE1-*Nnat*-FLAG	This paper
pT7CFE1-*Gfp*	Thermo Scientific (Pierce)
Probes for RT-PCR (TaqMan, Applied Biosystems, mouse unless otherwise stated)	
Nnat	Mm00440480_m1
Hprt	Mm00446968_m1
Cyclophilin A	Mm03302254_g1
Glut2	Mm00446224_m1
Neurod1	Mm01280117_m1
Ins2	Mm00731595_gH
Pdx1	Mm0435565_m1
Nkx6.1	Mm00454962_m1
Blcap	Mm00727119_s1
Atf6	Mm01295317_m1
Grp78	Mm00517691_m1

Chop	Mm00492097_m1
Xbp1s	Mm03464496_m1
Nnat (rat)	Rn00822063_m1
Sec11a (rat)	Rn00581878_m1
Hprt (rat)	Rn01527840_m1